TECHNICAL REPORT No. 60

AN EVALUATION OF THE PERFORMANCE OF THE ECMWF OPERATIONAL FORECASTING SYSTEM IN ANALYSING AND FORECASTING TROPICAL EASTERLY WAVE DISTURBANCES.

PART II: SPECTRAL INVESTIGATION

R.J. Reed*, E. Klinker and A. Hollingsworth

*Permanent Affiliation:
Department of Atmospheric Sciences
University of Washington Seattle,
Washington, U.S.A.

January 1987

Abstract

In Part I of this study synoptic methods were used to evaluate the performance of the ECMWF system in analysing and forecasting easterly wave disturbances over Africa and the Tropical Atlantic during August-September 1985. In this second part of the study, standard spectral methods are employed for the purpose of confirming and extending the previous results.

Important climatological features such as the southwest monsoon, trade winds, ITCZ, African Easterly Jet and Tropical Easterly Jet are well depicted by the time mean fields despite the data deficiencies documented in Part I. Spectra of time series of the 850 mb meridional wind along 18°N and 9°N reveal that the most prominent spectral peaks occurred in the 0.2 - 0.3 d^{-1} frequency band in agreement with the 3-5 day period found in Part I and in many other studies.

Patterns of the 850 mb and 700 mb vorticity variances in the 3-5 day wave band suggest disturbance tracks and regions of wave origin that are in agreement with the synoptic findings. The energetics implied by the covariances of temperature with the meridional and vertical wind components support the view that the waves owe their origin, at least in part, to baroclinic instability of the African Easterly Jet. Evidence was also found of a substantial barotropic energy conversion associated with a pronounced positive momentum flux at middle levels equatorward of the African Easterly Jet.

Inter-annual variations in the location of the maxima of the wave variances and covariances are believed to be real. The three dimensional wave structure was examined in detail and compared with the wave structure observed during GATE. The analysed structures resemble closely the structures documented by GATE investigations.

Cross spectrum analysis between time series of analysed and 48 hr forecast 850 mb meridional winds confirmed the finding of Part I that the forecast waves tended to be slower than the analysed waves, by about 150 km for a longitudinal displacement of 1400 km.

CONTENTS

1. INTRODUCTION

This report represents the second part of a two part series that examines the performance of the operational ECMWF forecasting system in analyzing and forecasting easterly waves over Africa and the tropical Atlantic during August-September 1985. The model is a spectral model with T106 resolution, Jarraud et al. (1985); the physical parameterisations are discussed in Tiedtke et al. (1987); the assimilation system is discussed in Shaw et al. (1987). The first part (Reed et al., 1987; hereafter called Part I) was essentially synoptic in nature. Large numbers of synoptic charts were used (1) to identify and track the waves that were present in the analyses, (2) to determine their average wavelengths, phase speeds and periods, and (3) to detect analysis problems arising from either characteristics of the analysis system or from data deficiencies. Evaluation of the forecast performance was based primarily on a daily sequence of 48 h forecasts of 850 mb vorticity.

The statistics compiled on the wave origins and tracks and on typical wave lengths, speeds and periods were consistent with results obtained in previous studies that looked at other years. Thus, it was concluded that the analysis system does a good job of representing the easterly waves. However, objective confirmation of these aspects of the synoptically determined wave characteristics is desirable. One of the aims of the present spectral study is to provide such confirmation.

A main finding regarding forecast performance was a tendency for the forecasted movement of the waves to be slightly slower than the observed movement. This finding is also amenable to objective verification by spectral techniques. A question regarding the forecasts that was not addressed in the synoptic study concerns how well the forecasts of various duration preserve the wave properties contained in the initial fields. Spectral information on the variance and covariance of forecasted wave fields will be examined as a means of answering this question. A further goal of this study is to provide information on the foregoing aspects of the forecast performance.

A final objective of the present study is to use spectral methods to define the three-dimensional structure of the waves and to compare the structure with that observed during Phase III of the Garp Atlantic Tropical Experiment (GATE). Data gathered by a special ship network allowed the wave structure to

be defined more accurately and thoroughly during the GATE period than has been possible before or since. Though multi-level maps were prepared in the companion synoptic study, no attempt was made to use these for defining wave structure.

The methodology employed in this report is described in the next section. In section 3 the time-mean fields that existed during the period of study are documented. These fields are of interest because they define the large scale environment within which the waves formed and travelled. Section 4 is devoted to an objective determination of the mean wavelength, propagation speed and period. Variance and covariance statistics that illuminate various aspects of the wave characteristics and behaviour are presented in section 5. Section 6 contains the spectrally determined wave structure and the comparison of the wave structure with that observed in GATE. The determinations of the systematic error in the forecasted wave movement and of the change in the statistical properties of the waves with the length of the forecast period are found in section 7. Concluding remarks appear in section 8.

2. DATA AND METHODS

The data used in this study are gridded data for August-September 1985, extracted from the ECMWF analysis and forecast archive. For technical reasons, a record length of 112 observational periods of one-half day length (56 days total) was employed instead of the full two month period. The quality of the data in the region of interest is discussed in Part I where it was noted that insufficient low-level winds were available east of 10°E to define any waves that might have been present.

The methodology is the same as in Klinker and Capaldo (1986). In the procedure to generate gridpoint data from archived spherical harmonics the first 40 wavenumbers were projected on a 3 by 3 latitude-longitude grid. Time series of geopotential, temperature, zonal wind, meridional wind, vertical wind and specific humidity at each gridpoint were then spectrally analysed. The Fast Fourier Transform method was used to calculate the power spectrum and the cross-power spectrum. From the co-spectrum and quadrature spectrum phase differences and coherences between points separated in the vertical or in the horizontal have also been calculated. As the time series consists of 56 twice daily analyses (00 GMT and 12 GMT), the basic spectral interval is one cycle per 56 days. In the representation of power spectra at selected points the spectrum is smoothed by a 1/4, 1/2, 1/4 filter (Hann window). For the investigation of the wave structure in the period range of around 3 to 5 days the spectral values were integrated over the appropriate number of intervals.

From the time series containing 56 twice daily spherical harmonics time means were calculated. Most mean fields were calculated from spherical harmonics representing 40 waves, except that fields of divergence, vorticity and vertical velocity were calculated from 21 waves to suppress undesired noise.

3. MEAN STATE

In this section we present time-mean fields of various meteorological parameters for August-September 1985 based on twice daily (0000 and 1200 GMT) initialised analyses. The discussion will be brief with emphasis on features that are believed to influence wave development and behaviour.

3.1 Horizontal maps

The flow fields at 1000 mb, 850 mb, 700 mb and 200 mb are depicted in Figs. 1a-d. Main features of interest at 1000 mb (Fig. 1a) are:

(1) The southwesterly monsoon flow over central and West Africa south of 20°N that originates in the trades of the South Atlantic,

(2) The northeasterly harmattan over the Sahara,

(3) The zone of confluence (and convergence) of these currents near 20°N in what is generally referred to as the monsoon trough or intertropical convergence zone (ITCZ),

(4) The northeasterly trade winds over the Atlantic and Caribbean with speed maxima west of North Africa and in the Caribbean.

The shallowness of the African monsoon is evidenced by its near disappearance at the 850 mb level (Fig. 1b). The harmattan extends further southward at this level (ITCZ displaced southward), overriding the low-level monsoon flow. The trades are weaker in the northeast Atlantic and somewhat stronger in the Caribbean.

A new feature of importance appears at 700 mb (Fig. 1c): an east-west jet stream extending from central Africa to the central Atlantic with axis near 15°N. We will refer to this jet as the African Easterly Jet (AEJ). The reversal from low-level westerlies to mid-level easterlies in the sub-Saharan region is indicative of a westward directed thermal wind and hence of the existence of warmer temperatures over the Sahara than over the wetter and cooler land area and cooler ocean to the south.

Features of particular interest at 200 mb (Fig. 1d) are the Tropical Easterly Jet (TEJ) that extends from the Gulf of Aden to the northern coast of the Gulf of Guinea and the mid-ocean trough that appears near 45°W in subtropical latitudes. A weak west to southwesterly subtropical jet is located ahead of

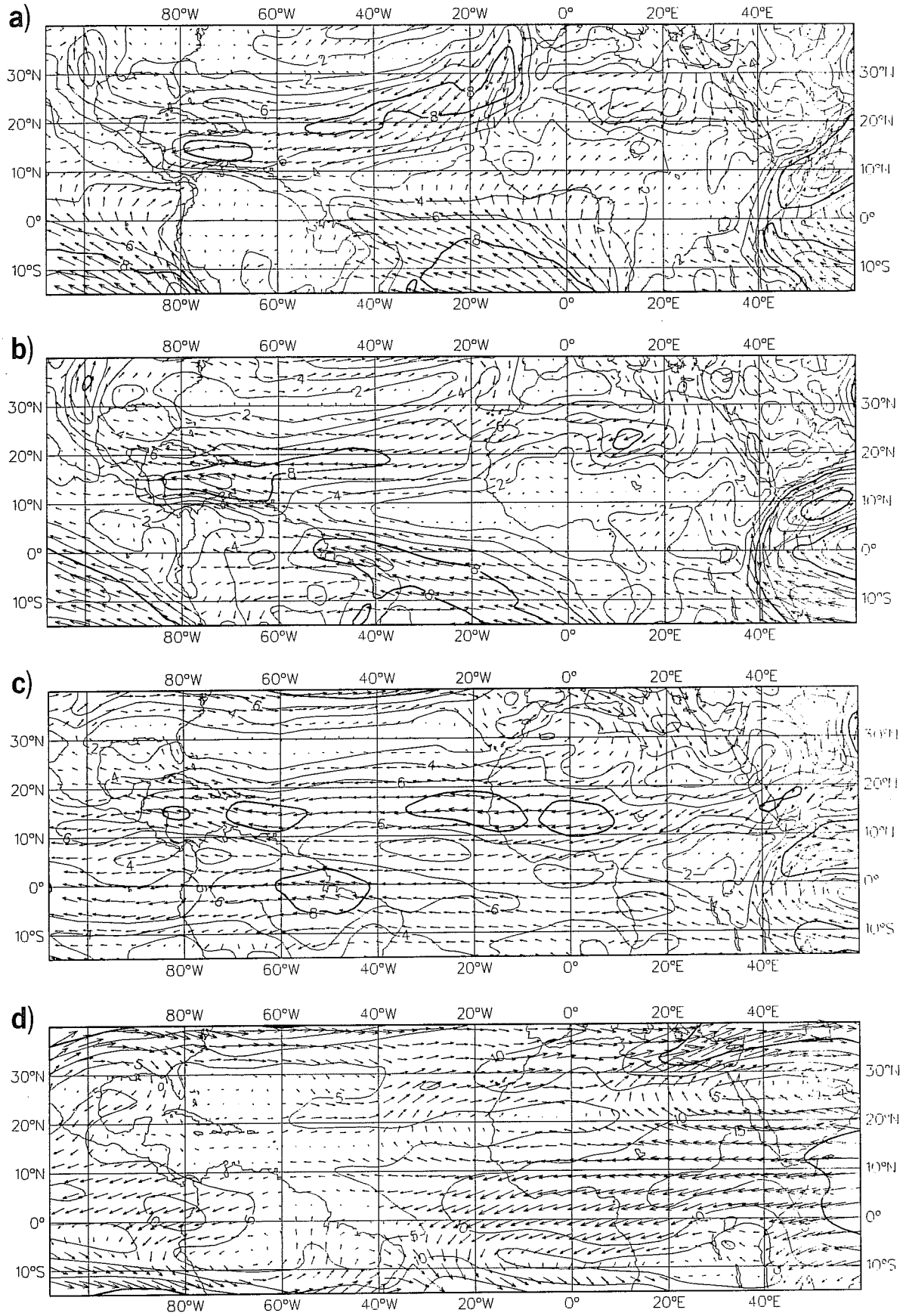

Figure 1 Average wind speed (contours) and direction (arrows), August-September 1985, at (a) 1000 mb, (b) 850 mb, (c) 700 mb and (d) 200 mb.

(to the east of) the trough. The sub-tropical jet lies almost directly over the northeast trades, signifying enhanced tropospheric baroclinity in the region.

The low to mid-level vorticity fields and low-level divergence field are of interest in connection with the origin and maintenance of the waves. These fields are shown in Figs. 2a-c. Cyclonic vorticity prevails at 850 mb (Fig. 2a) in the region of wave origin over Africa between 10°N and 20°N (see Fig. 1e of Part I). The belt of positive vorticity is displaced slightly southward in the central and eastern Atlantic and much further southward in the western Atlantic and Caribbean. At 700 mb (Fig. 2b) the band of cyclonic vorticity is displaced 5-10 degrees further south over the continent than at 850 mb, an indication of the southward slope of the monsoon trough with elevation. Over the ocean the position of the band is approximately the same at the upper level as at the lower.

In many ways the 1000 mb convergence pattern (Fig. 2c) parallels that of the 850 mb vorticity. Over much of Africa the axis of maximum convergence, or ITCZ, is situated near 20°N. An abrupt southward shift occurs near the coast so that over the eastern and central Atlantic its location is near 12°N. Further west its position is near and somewhat south of the vorticity maximum.

Fields of specific humidity at four levels (1000, 850, 700 and 500 mb) are shown in Fig. 3. The 1000 mb pattern over Africa is quite striking (Fig. 3a). Elongated regions of very high and very low specific humidity extend east-west across the continent, their axes separated by only about 10° of latitude. The moist axis lies close to, or slightly north of, the axis of the climatological rainfall maximum (Thompson, 1965). The dry axis lies over the Sahara. The moist axis shifts slightly southward aloft. The dry region becomes less pronounced with height and retreats northward to the Mediterranean (Figs. 3b-d). A tongue of moister air protrudes northward to the Atlas Mountains.

Moisture gradients at the surface are very weak over the ocean. Aloft the moisture differences are greater with quite large mixing ratios occurring at 850 mb near 11°N and quite low values at 28°N (Fig. 3b).

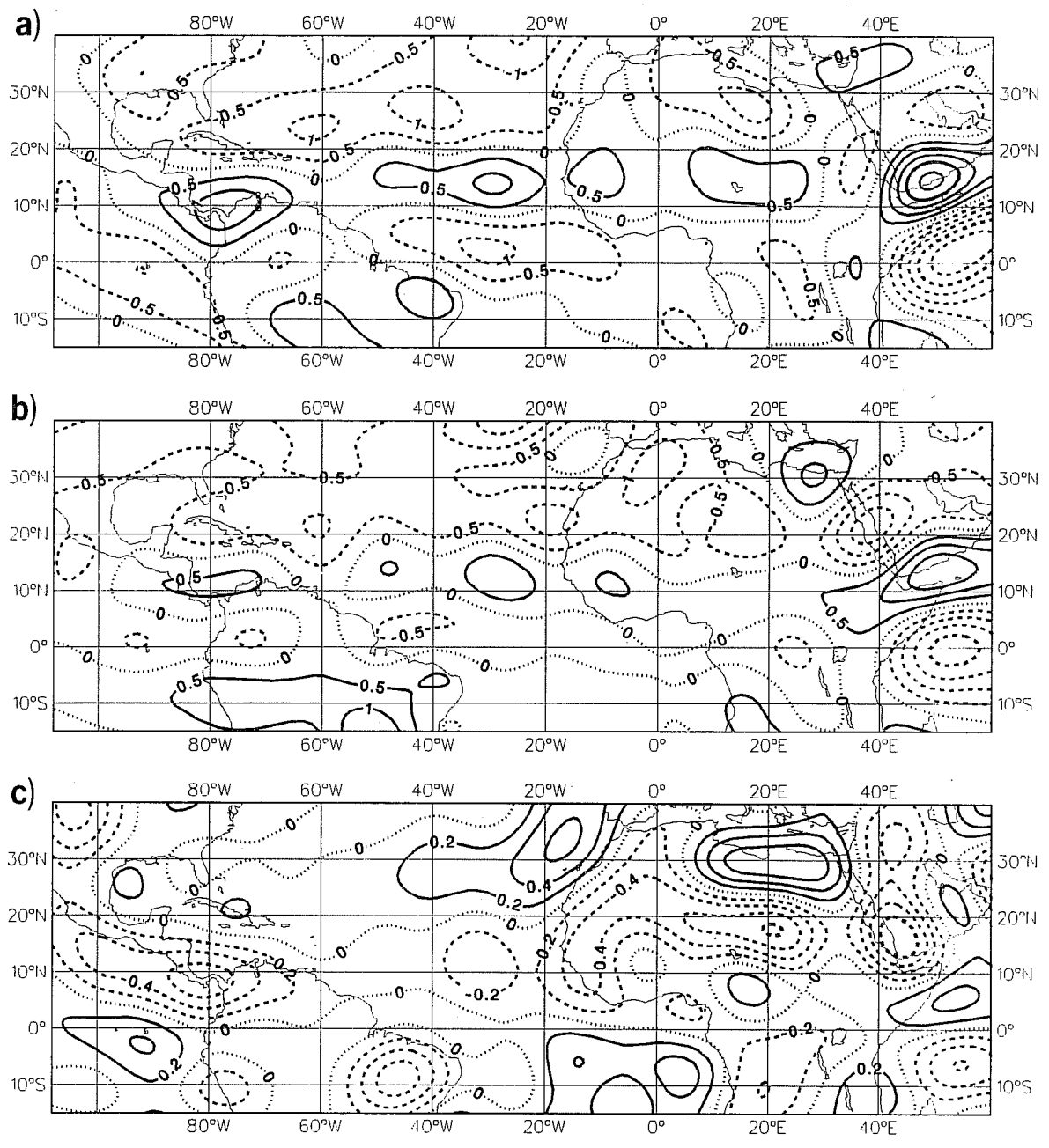

Figure 2 (a) Average vorticity (10^{-5} s^{-1}) at 850 mb, August-September 1985, (b) at 700 mb and (c) average divergence (10^{-5} s^{-1}) at 1000 mb for the same period.

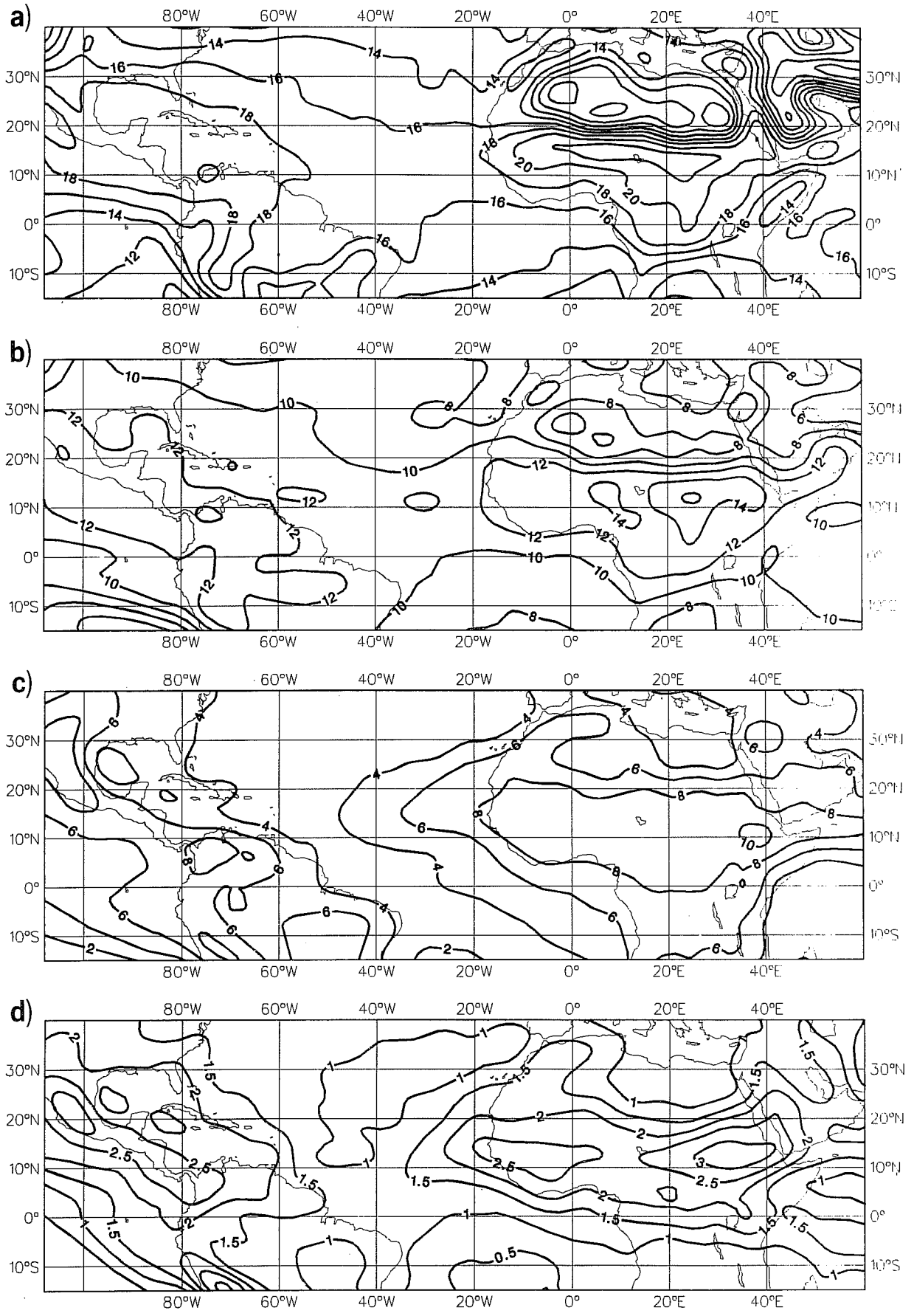

Figure 3 (a) Average specific humidity (q), August-September 1985, for (a) 1000 mb, (b) 850 mb, (c) 700 mb and (d) 500 mb; units are g/kg.

3.2 Vertical cross sections

These are displayed along four meridians, 40°W, 20°W, 0° and 20°E, for the two wind components (u,v) vertical motion (ω), divergence (D), vorticity (ζ), temperature (T) and specific humidity (q). A number of features mentioned above are evident in the zonal wind section (Fig. 4). The low-level westerlies centred between the equator and 10°N in Figs. 4b-d represent the monsoon flow. Their maximum upward extent is to 750 mb (Fig. 4d). The harmattans can be seen between 20°N and 30°N in Figs. 4c and d, and the speed maxima of the northeasterly and southeasterly trades can be seen at 20°N and the equator, respectively, in Fig. 4a. The AEJ appears as a distinct core of enhanced easterlies centred near 15°N and 600 mb in Figs. 4b and c and as an elongated tongue in Fig. 4d. The maximum speed of somewhat less than 10 ms^{-1} is weaker than found in other studies (e.g. Burpee, 1972; Reed et al., 1977). The monthly mean reported winds for August were weaker than normal, while the monthly means for September were near normal.

Features evident in Fig. 4 that have not previously been mentioned are the easterly jet near 200 mb and 0°-10°N in Figs. 4b-d and the high level westerly jet that appears near 22°N in Fig. 4a and between 30°N and 35°N in the other sections. The easterly jet is an extension of the well known jet stream that forms over the Indian Ocean during the summer monsoon and is sometimes referred to as the Tropical Easterly Jet (TEJ). The westerly jet originates at low latitudes ahead of the oceanic upper-tropospheric trough and increases in strength as it approaches and enters the Mediterranean.

Cross sections of the meridional wind component appear in Fig. 5. Evident near the surface are the southerly components of the African monsoon (Figs. 5b-d) and southeast trades (Fig. 5a) and the northerly components of the harmattan (Figs. 5c and d) and the northeast trades (Figs. 5a and b). Other prominent features are the high-level northerly and southerly components associated with the aforementioned upper easterlies and westerlies, respectively, and the mid-level northerlies seen near 10°-15°N in Figs. 5c and d. These perhaps, should be regarded as part of the harmattan, but their connection to the surface flow is not simple.

Divergences and corresponding vertical motions (omega) are depicted in Figs. 6 and 7 respectively. Over the ocean (Figs. 6a and b) shallow layers of

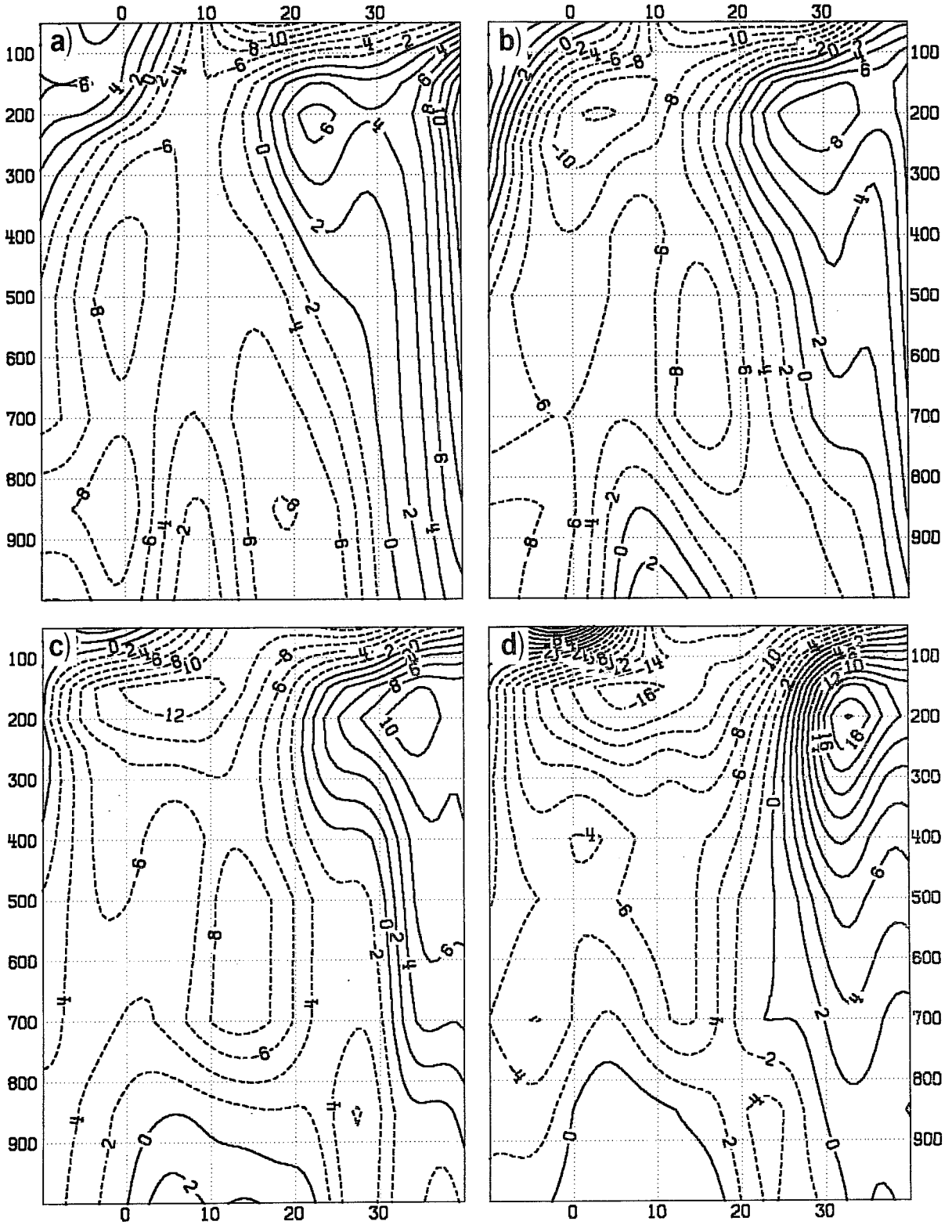

Figure 4 Meridional sections of mean zonal wind speed (m s^{-1}), August-September 1985, for (a) 40°W, (b) 20°W, (c) 0°, (d) 20°E.

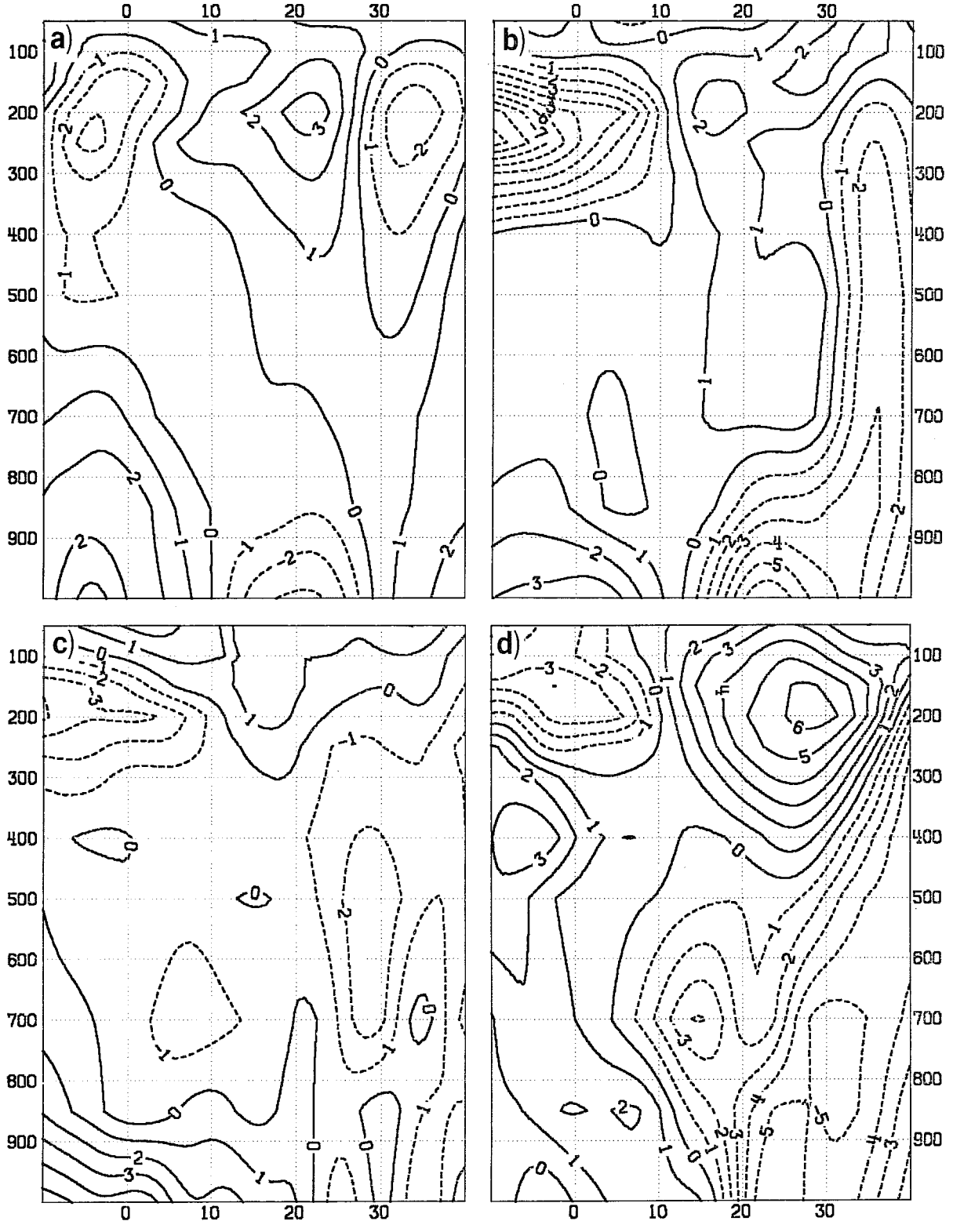

Figure 5 Same as Figure 4 for mean meridional wind speed.

convergence are seen next to the surface near 10°N surmounted by thin layers of divergence centred between 250 and 200 mb. As required by mass continuity, ascending motion occurs in the column (Figs. 7a and b). At 40°W, for reasons that are not understood, the upper divergence region is displaced about 5 degrees south of the maximum surface convergence so that the vertical motion field tilts and weakens rapidly with height. Pronounced sinking motion and low level divergence occur over the ocean at 30°N and 10°S (Figs. 6b and 7b). Viewed in conjunction with Figs. 5a and b, the foregoing figures yield a picture of an almost ideal Hadley circulation with inflow from north and south in the boundary layer, rising motion above, outflow in the upper troposphere and sinking motion on the flanks.

Over the African continent the picture is more complex (Figs. 6c and d and 7c and d). Strong upper-level divergence (Figs. 6c and d) still occurs between 5°N-10°N, but the low-level convergence is shifted northward to the vicinity of 20°N, the position already noted in earlier mention of the ITCZ. The convergence over land is deeper than over the ocean and is surmounted by a separate mid-level region of divergence. Accordingly the vertical motion field (Figs. 7c and d) exhibits separated lower level and upper level regions of maximum upward motion. The dual structure may arise because, unlike over the ocean where only a single zone of heating occurs in association with latent heat release in the ITCZ, over land both latent heat release in the rain belt near 10°N and sensible heating in the deep convective boundary layer over the Sahara contribute to upward motion.

The vorticity fields appear in Figs. 8a-d. In general they show a deep region of cyclonic vorticity that is centred between 15°N and 20°N at the surface and that slopes southward with height, particularly at the prime meridian. This zone is flanked on either side by regions of anticyclonic vorticity.

Figures 9a-d depict the temperature field. At 40°W (Fig. 9a) two maxima exist at low levels, one over Brazil and a weaker one that slopes upward from 10°N at the surface to near 20°N at 800 mb. The surface warmth is associated with the sea surface temperature maximum (not shown) and the 800 mb warmth with the advection of warm air from the African continent. At middle and upper levels warmest temperatures occur near 10°N, probably an outcome of latent heat release in convection. The picture in the eastern Atlantic (Fig. 9b) is

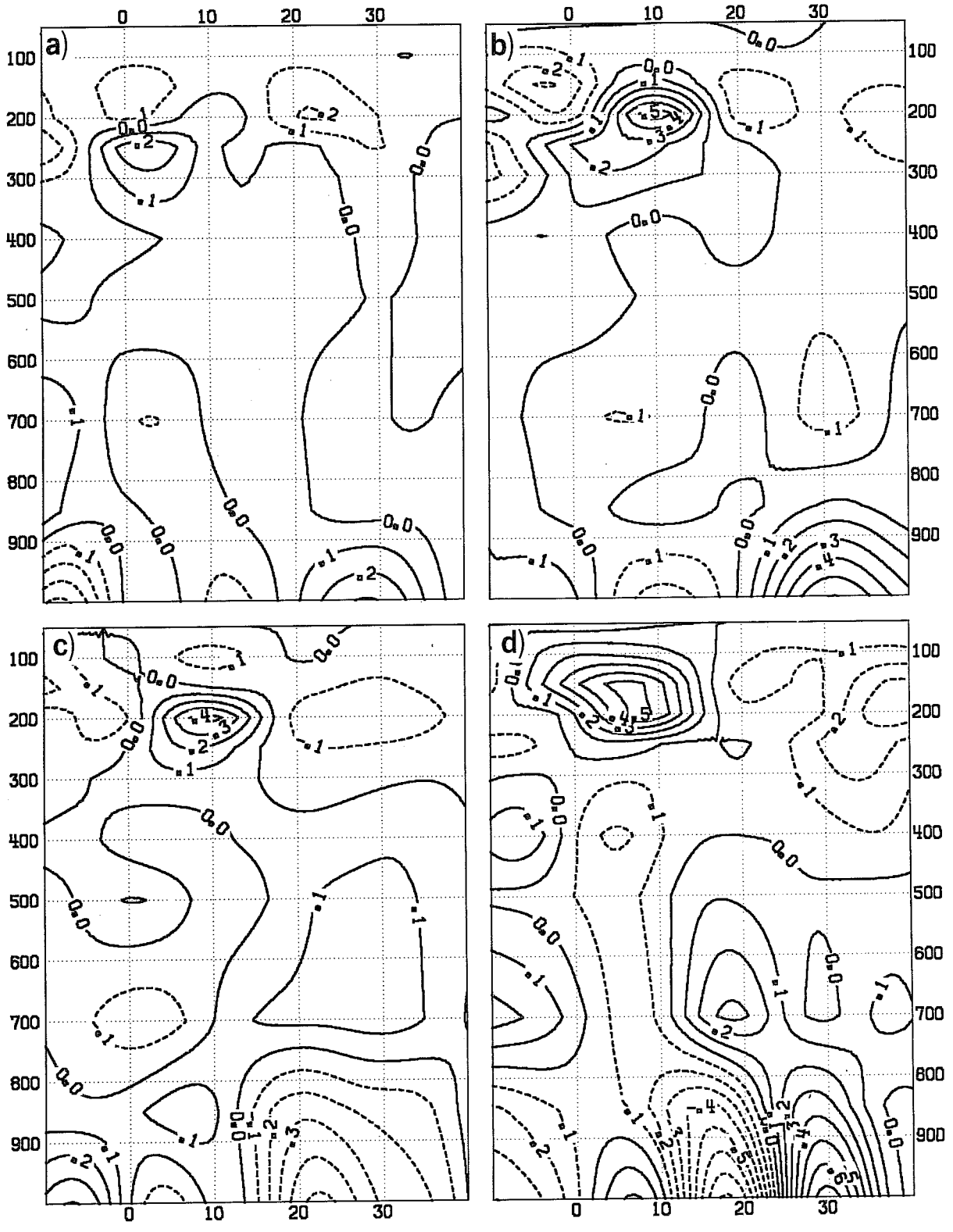

Figure 6 Same as Figure 4 for horizontal divergence (10^{-5} s^{-1}).

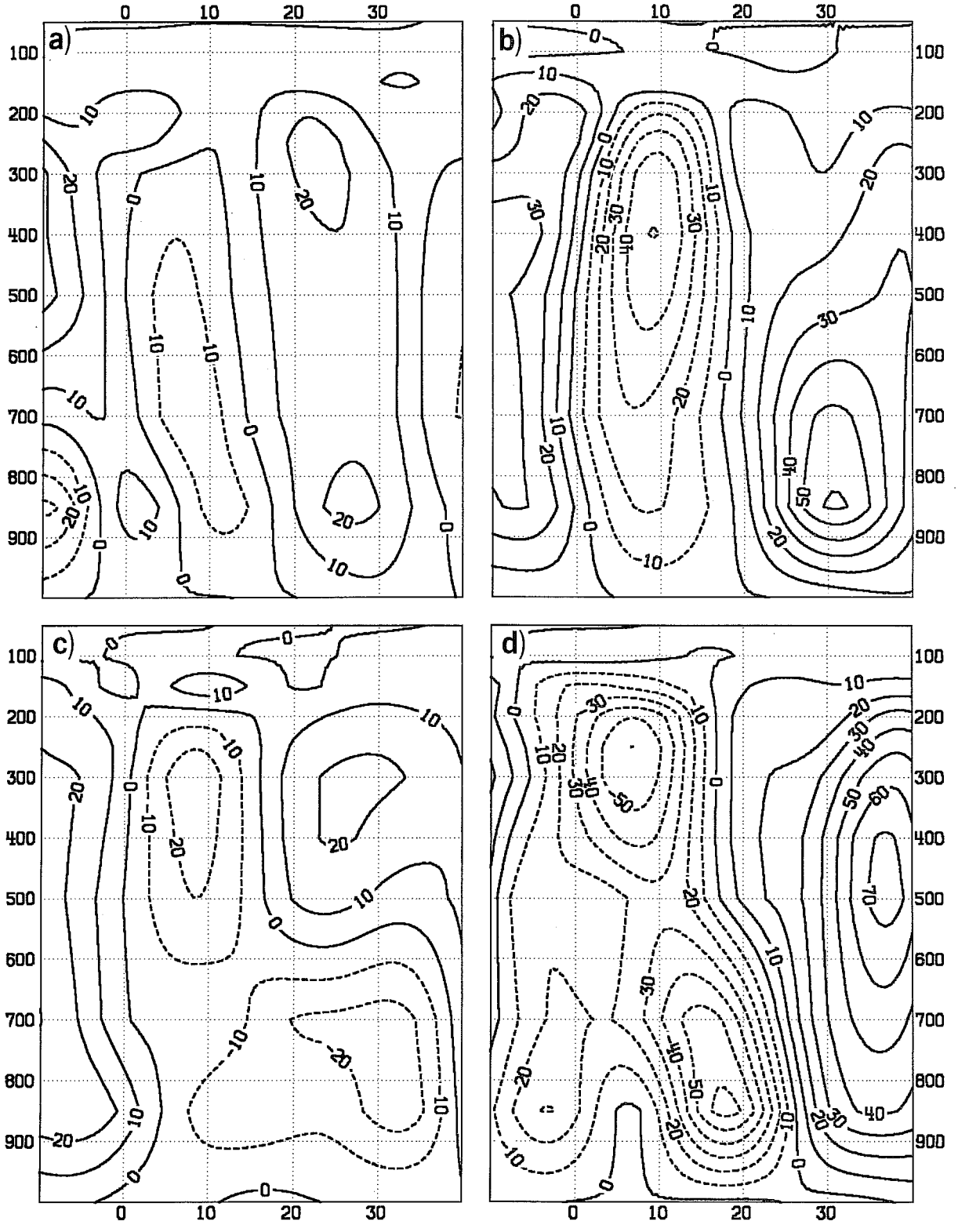

Figure 7 Same as Figure 4 for vertical velocity (10^{-3} Pa s^{-1}).

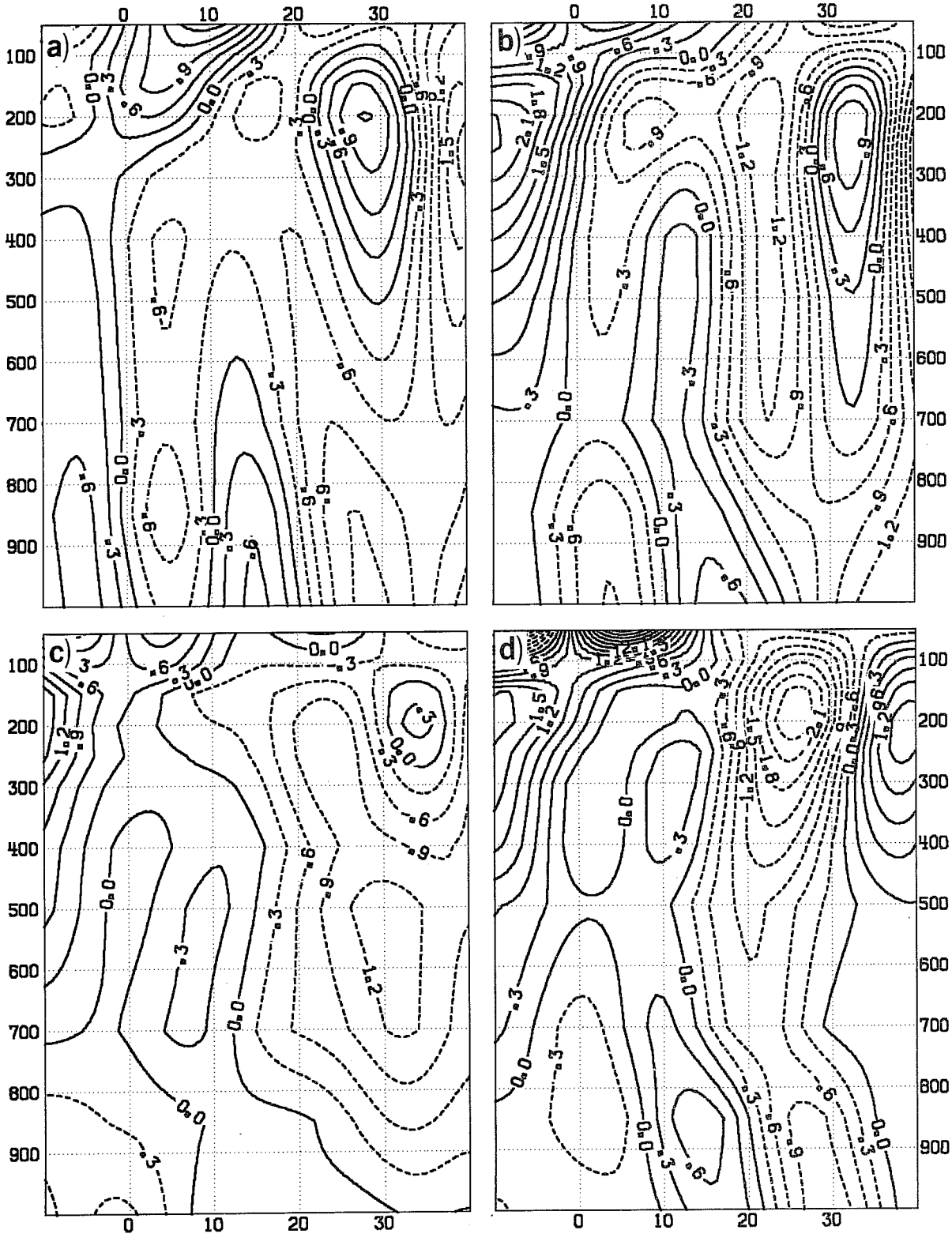

Figure 8 Same as Figure 4 for relative vorticity (10^{-5} s^{-1}).

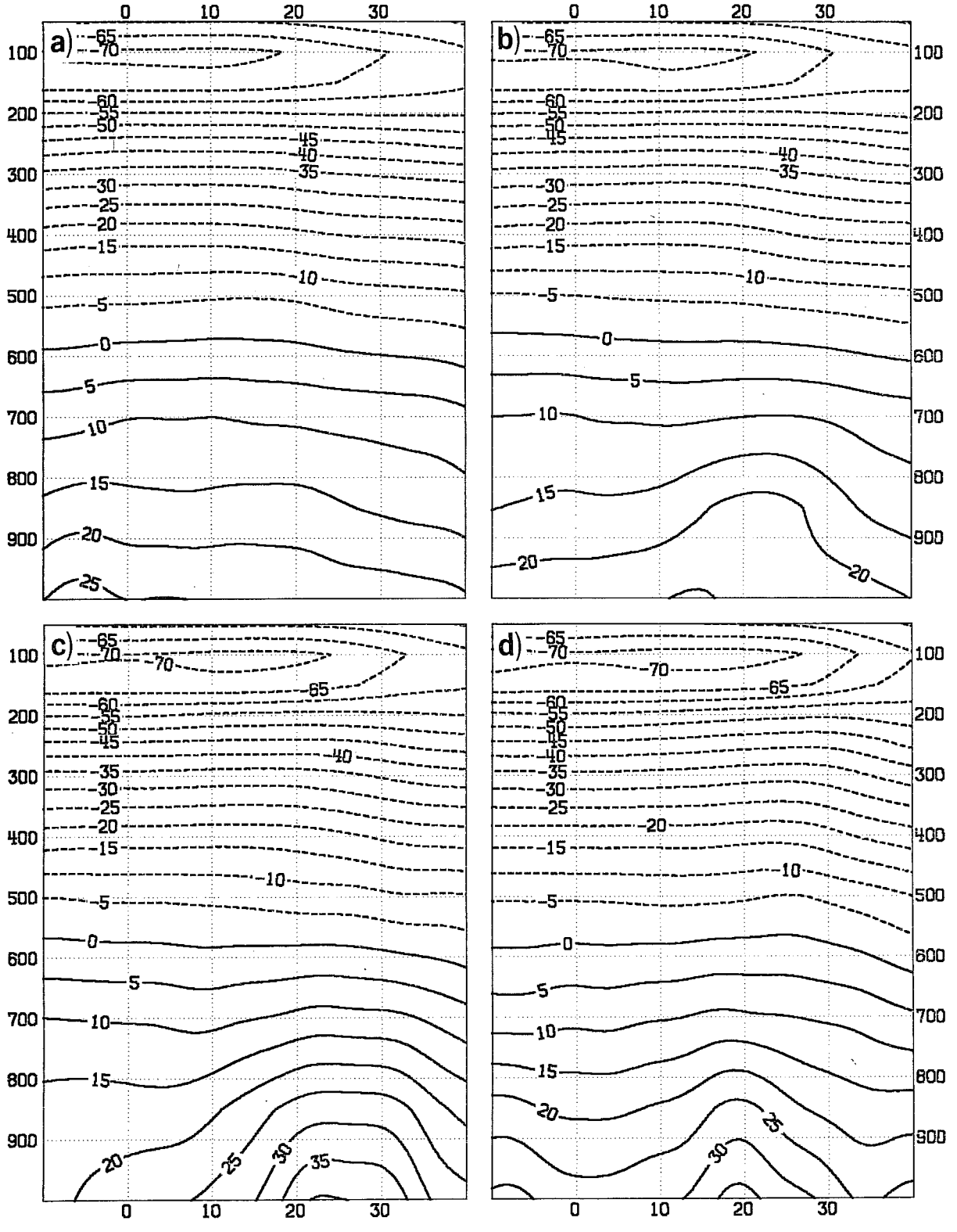

Figure 9 Same as Figure 4 for temperature (°C).

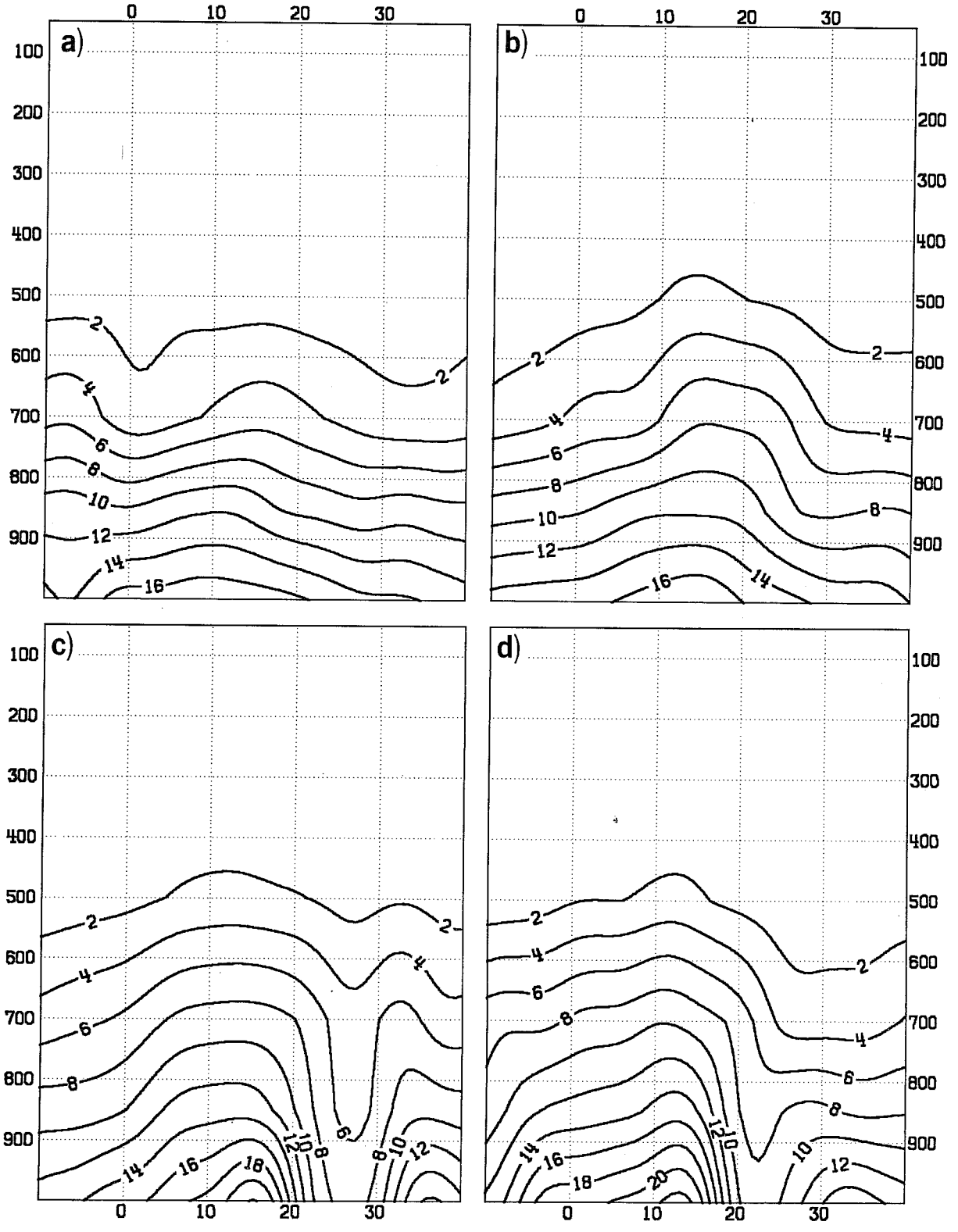

Figure 10 Same as Figure 4 for specific humidity (10^{-3}).

qualitatively the same as that further west except that the warm zone produced by continental heating over Brazil is lacking.

Over the African continent the most prominent feature is the warm region over the Sahara (Figs. 9c and d). This extends to about 500-600 mb. Higher up the maximum warmth shifts southward at the prime meridian and northward at 20°E. These upper maxima are probably associated with patterns of subsidence and advection that are not easily described.

Finally, cross sections of moisture are presented in Figs. 10a-d. Features of note are the strip of large specific humidity centred at 10°-12°N and the region of minimum specific humidity over the desert near 25°N. The moist strip coincides with the rainfall maximum, and the moisture content increases from ocean to continent. The dry region is clearly a consequence of the strong subsidence seen near 30°N on Fig. 7d. The air is obviously well mixed below 700 mb by the time it reaches the prime meridian (Fig. 10c). The existence of thorough mixing to near 500 mb in the Saharan air layer (SAL) is well documented (Carlson and Prospero, 1972) so that it seems likely that the analyses systematically overestimate the specific humidity and underestimate the lapse rate between 700 and 500 mb. According to Carlson and Prospero, typical moisture contents in the deep mixed layer are 4 g kg^{-1} or less, suggesting that the analyses do not depict the extreme dryness of the desert air.

4. BASIC WAVE PARAMETERS

We use this term to denote the period, wavelength and propagation speed or phase speed of the easterly waves. The results of Part I on the identification and tracking of individual waves for August-September 1985 indicated that the average period over Africa and the central and eastern Atlantic was about 3 1/2 days, the average wavelength was in the range 1900 km to 2800 km and the phase speed was in the range 6°-7° longitude per day. These figures agree well with the results of earlier studies.

A number of investigators have employed spectral techniques to determine the basic wave parameters. Yanai et al., (1968) used them in connection with easterly waves in the Pacific while Burpee (1972), Viltard and de Félice (1979) and Albignat and Reed (1980) used them in connection with African waves. It is of interest to apply these techniques to the waves as analysed during the August-September period. The wave period will be determined from power spectra of the analysed 850 mb meridional wind component taken at various locations. As stated previously winds used in the spectrum analysis are initialised winds at the model grid points, not station winds. The wave length will be obtained from cross spectrum analysis in the manner introduced by Yanai et al., (1968).

Figure 11 shows power spectra along 18°N at 3 degree intervals of longitude from 18°E to 39°W. The prominent peak at a period of approximately 4 days is immediately evident. The 4-day wave first appears near 12°E and increases rapidly in amplitude westward, reaching its maximum intensity in the region between the prime meridian and the coast (15°W). Its amplitude diminishes over the Atlantic, but the 4-day wave is still detectable at 39°W as one component of a double spectral peak. The second component at a period of 5-6 days, is believed to be the signature of low-level perturbations, that form in connection with upper tropospheric developments in or near the mid-ocean trough (Simpson et al., 1968). Spectra extending further westward (not shown) reveal that the 4-day wave of African origin maintains its strength to at least 60°W whereas the 5-6 day wave rapidly fades away.

Additional peaks of interest are seen in Fig. 11 at periods of 3-3.5 days near the prime meridian and at 2.5-3 days near the coast. The origin of these peaks is obscure. From the companion synoptic study it seems doubtful that

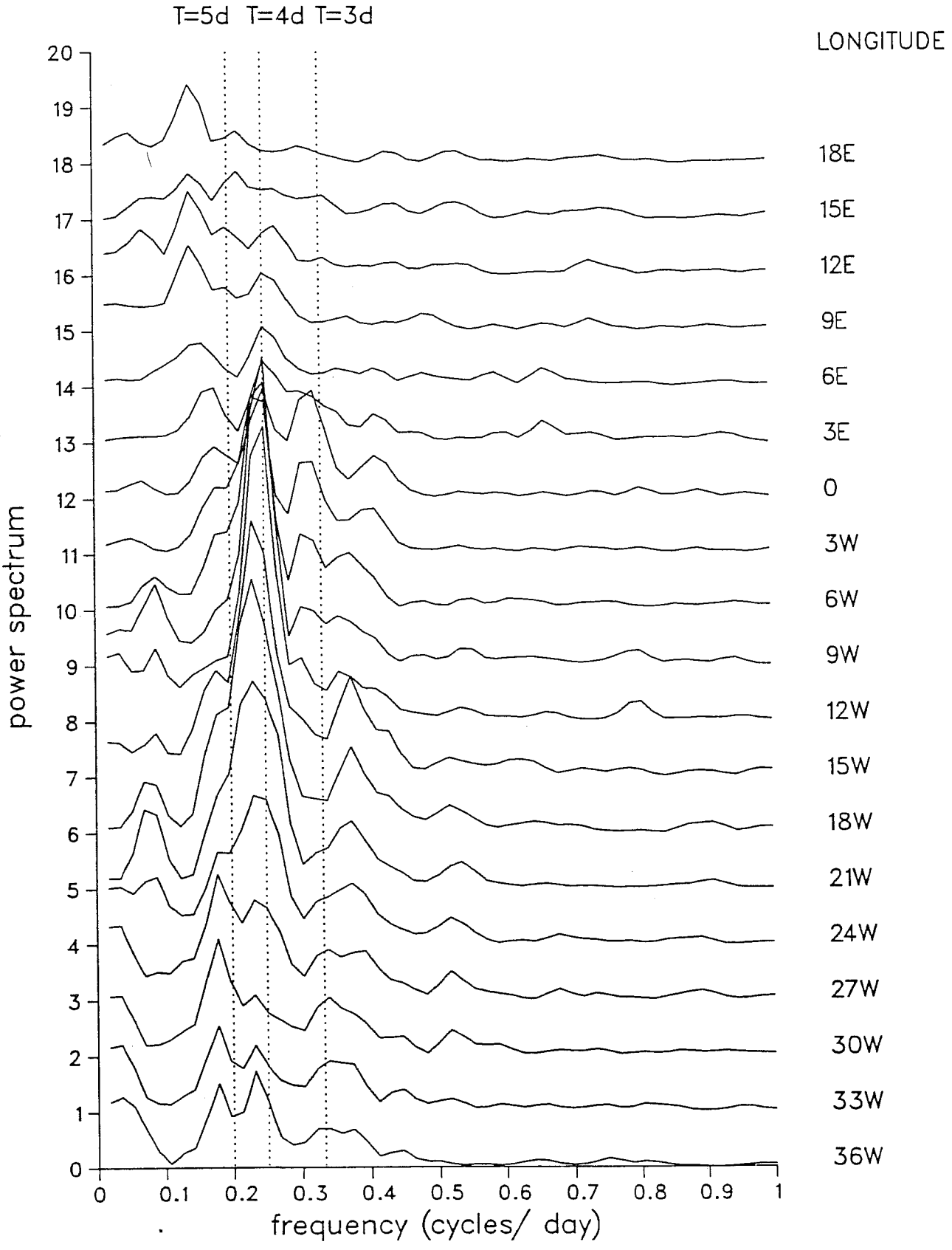

Figure 11 Power spectra of 850 mb meridional wind component along 18°N between 18° and 39°W. Vertical dotted lines indicate periods in days.

they are associated with phenomena distinct from the basic African wave. Individual waves are seen to vary in frequency and intensity and to follow somewhat different paths so that spectra for limited time periods cannot be expected to exhibit single, sharp peaks even though only one type of wave is present.

Wave spectra for 9°N are shown in Fig. 12. Again the most prominent feature is the basic 4-day wave which at this latitude first appears at 3°W. Peak intensity is again attained in the vicinity of the coast. A gradual decrease in intensity occurs over the ocean, though a weak peak, somewhat shifted toward higher frequency, still remains at 39°W. This peak is traceable almost to the South American coast (57°W) on spectra extending further to the west (not shown). The 3-3.5 day peak is even more pronounced at this latitude than at 18°N and first makes its appearance at 9°E. The 2.5-3 day and 5-6 day peaks are virtually absent. Further comment regarding the dual 4 day and 3-3.5 day peaks in Fig. 12 will be made when discussing Fig. 20, which depicts the geographical distribution of the 850 mb total meridional wind variance for oscillations with periods in the 3 to 5 day range.

Figure 13 depicts for the 2.9-5.1 day frequency band the average difference in phase between the time series of the 850 mb meridional component at 18°N, 15°W and at points on the same latitude circle but longitudinally separated by varying distances. Also shown are the coherences between the space-lagged time series. East of 15°W the phase difference is about 180° per 12° of longitude, yielding a wave length of approximately 2,500 km. The corresponding figures for west of 15°W are 180° per 13° of longitude and a wave length of 2700 km. The wave lengths are 4-500 km longer than found synoptically. Since the periods are roughly the same, the phase speeds are faster, being about 6.8° longitude d^{-1} to the east and 7.4° longitude d^{-1} to the west. Although perfect agreement is not obtained with the synoptic results, the agreement is sufficiently close to make further discussion unwarranted.

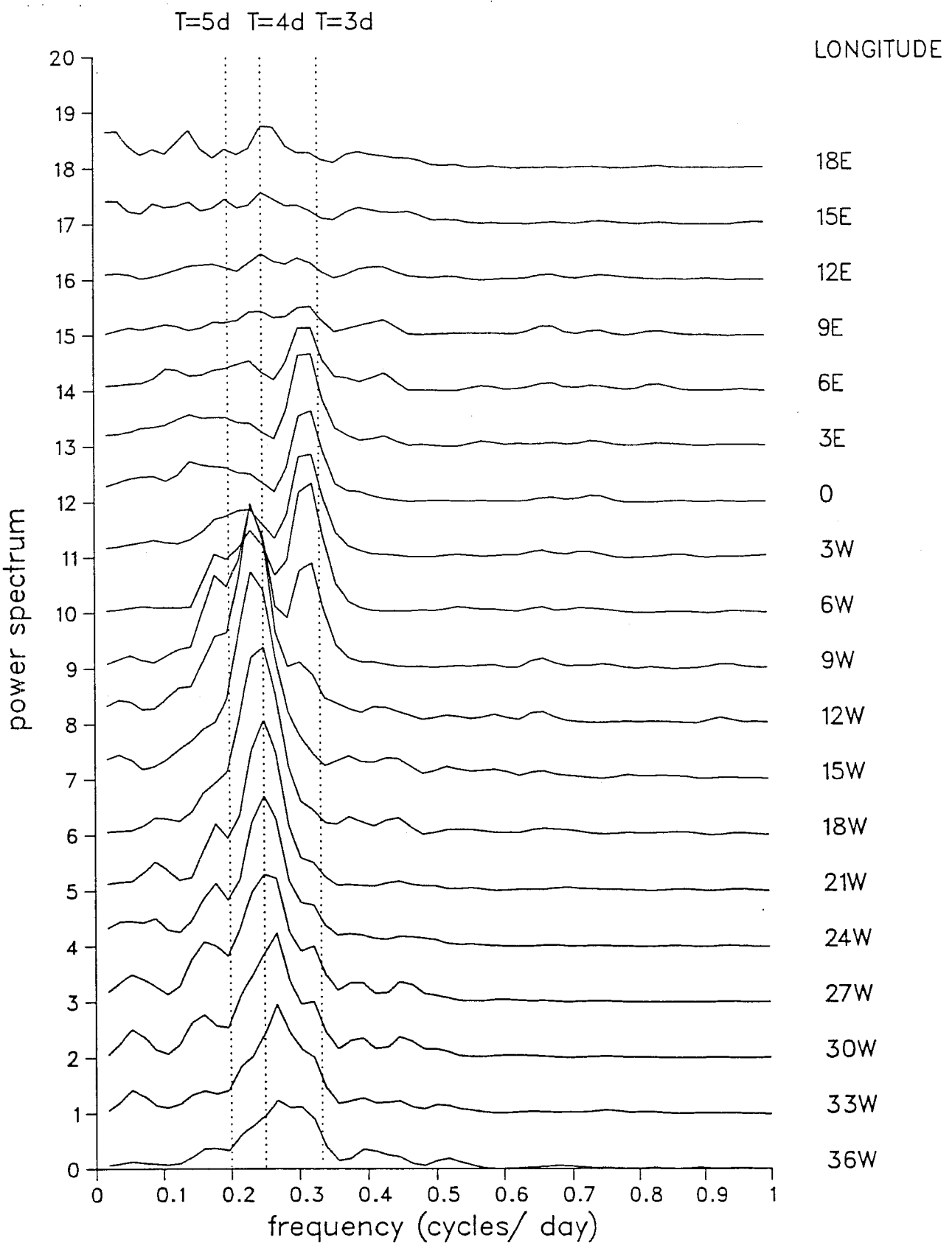

Figure 12 As in Figure 11 for 9°N between 18°W and 39°W.

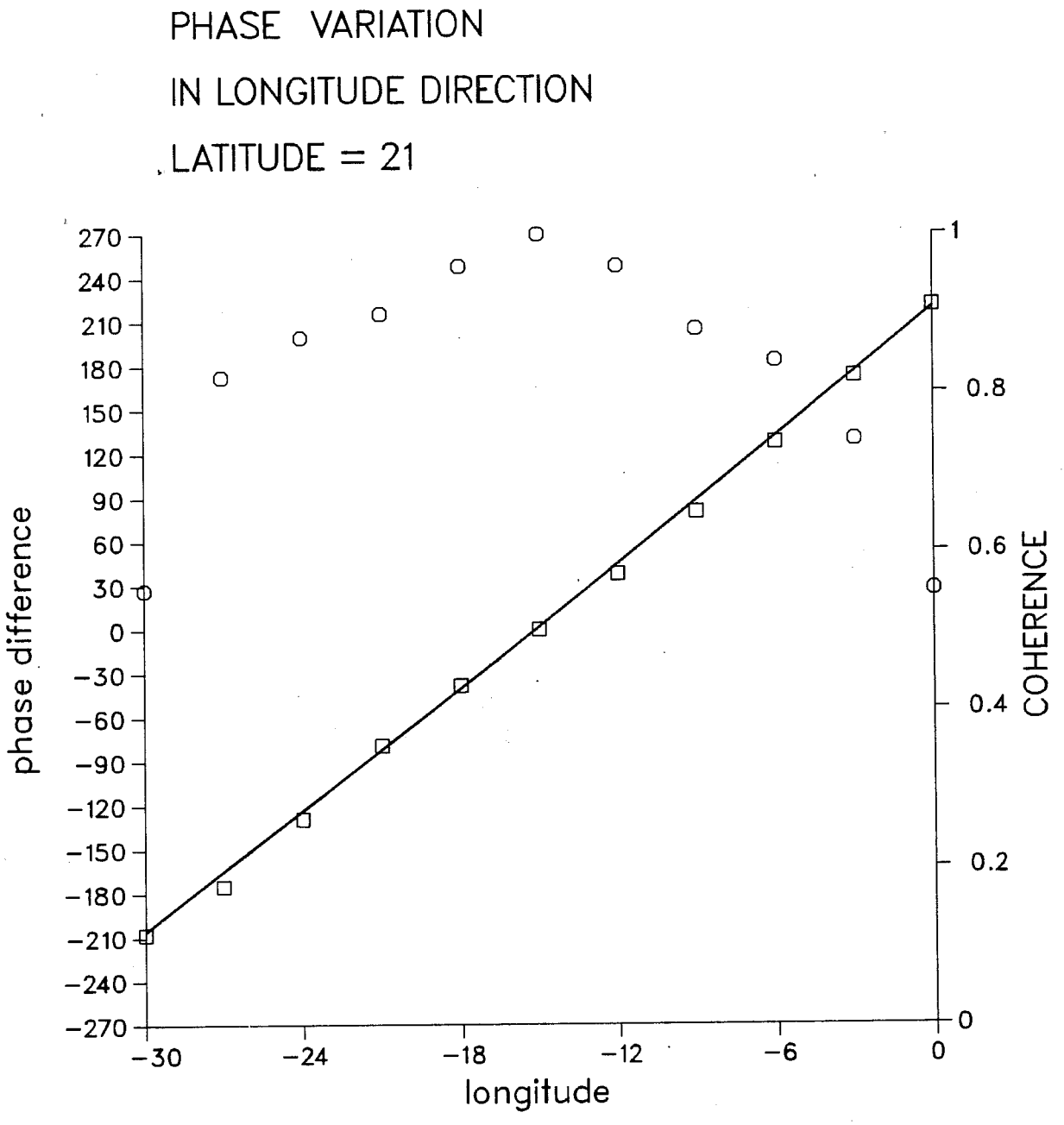

Figure 13 Phase difference (degrees) at 18°N between time series of meridional wind at 15°W and adjacent longitudes (squares). Coherences are shown by circles.

5. WAVE ACTIVITY AND BEHAVIOUR AS SHOWN BY VARIANCE AND COVARIANCE STATISTICS

In Fig. 1 of Part I maps were shown of the points of origin and paths of the 20 waves that occurred during August-September 1985. The tracks of the wave disturbances were determined mainly by following points of maximum vorticity at 850 mb, though account was also taken of 700 mb trough axes and METEOSAT cloud patterns. The origin of a wave was considered to be the position at which its vorticity centre first progressed westward at a speed of $\geq 3°$ longitude d^{-1}. Generally the vorticity was quite weak at the starting point.

As a check on the conclusions of Part I, charts have been prepared of the variance of vorticity in frequency bands corresponding approximately to the 3 to 5 day wave period. The primary wave tracks should appear as east-west strips of large variance on such charts, and the main regions of origin or growth as areas in which the variance begins to increase markedly in the direction of wave motion (westward). Nitta and Takayabu (1985) have previously used the vorticity variance to help define wave tracks and origins in the summer of 1979, while Burpee (1972) and Albignat and Reed (1980) have used the variance of the meridional wind component, also a measure of wave activity, to determine regions of origin in other years.

Maps of the 850 mb and 700 mb vorticity variances in the 3-4 day range appear in Figs. 14a and b, and a map of the 700 mb variance for a somewhat broader, roughly 3-5 day, range is shown in Fig. 14c. The pattern in Fig. 14a conforms well to the findings of the synoptic study. The axis of maximum vorticity, or the main wave track across the Atlantic, is situated between 15°N and 17°N, slightly north of the synoptically determined wave track. Main regions of origin are suggested near 20°N, 10°E and near 12°N, 0°-5°W in agreement with the synoptic results. The tendency for at least some of the waves to re-strengthen in the western Atlantic is also indicated.

The 700 mb variance pattern for the 3-4 day wave band is shown in Fig. 15b. Features seen in this figure agree most closely with the findings of the synoptic study. The southerly region of origin is displaced further to the east than on the corresponding 850 mb chart (Fig. 14a), and distinct storm tracks can be seen emanating both from this region and from the northerly region, merging into a single path in the eastern ocean. The track over the

ocean is still somewhat north of the synoptically derived path. The sensitivity of the variance field to a small increase of the frequency interval can be seen in Fig. 14c. Important additional features arising from broadening the band width are the prominent regions of large variance near 20°N, 15°W and near 25°N, 35°W. The origin of the first of these regions is obscure. It may arise from a temporary strengthening of some of the waves in connection with topographical peculiarities of the region: the sharp land-sea thermal contrasts and the proximity of the Atlas Mountains. The mid-ocean maximum is more easily explained as a likely manifestation of the 5-6 day waves found in the 850 mb meridional wind spectra (Fig. 11). These, it will be recalled, were identified with weak disturbances known to form in or near the mid-ocean upper-tropospheric trough (Simpson et al., 1968). One such disturbance was documented in Example 5 of Section 4.2 of the companion study.

An additional region of enhanced variance near 50°W in Figs. 14b and c may be caused by interactions of the African waves with the upper-tropospheric trough (Frank, 1969). The latter often extends southwestward to the region in question.

Further characteristics of the waves may be studied with other charts of variances and covariances. A selection of these appear in Figs. 15a-d and 16a-d. The variance of the meridional wind component (Fig. 15a) resembles that of the vorticity (Fig. 14a) in broad aspect, but some noteworthy differences exist. The southerly variance maximum is displaced westward and southward to a location over the ocean. The Atlantic "storm track" is displaced to the north. The vorticity chart appears to give a better representation of the synoptically observed behaviour. The appearance of such a prominent maximum at 6°N, 18°W requires explanation. It may be associated with wave-induced pulsations of the monsoon flow that are better related to the deformation of the wind field than to the vorticity.

The temperature variance (Fig. 15b) is large over the Sahara and downwind of the Sahara in the region of coastal temperature contrast. The vertical velocity variance (Fig. 15c) is large along the axis of enhanced vorticity (Fig. 14a) that defines the northern storm track. A lobe of enhanced variance protrudes southward near 10°W. This lobe is almost certainly associated with the vorticity maximum that appears along the southern track (Fig. 14a).

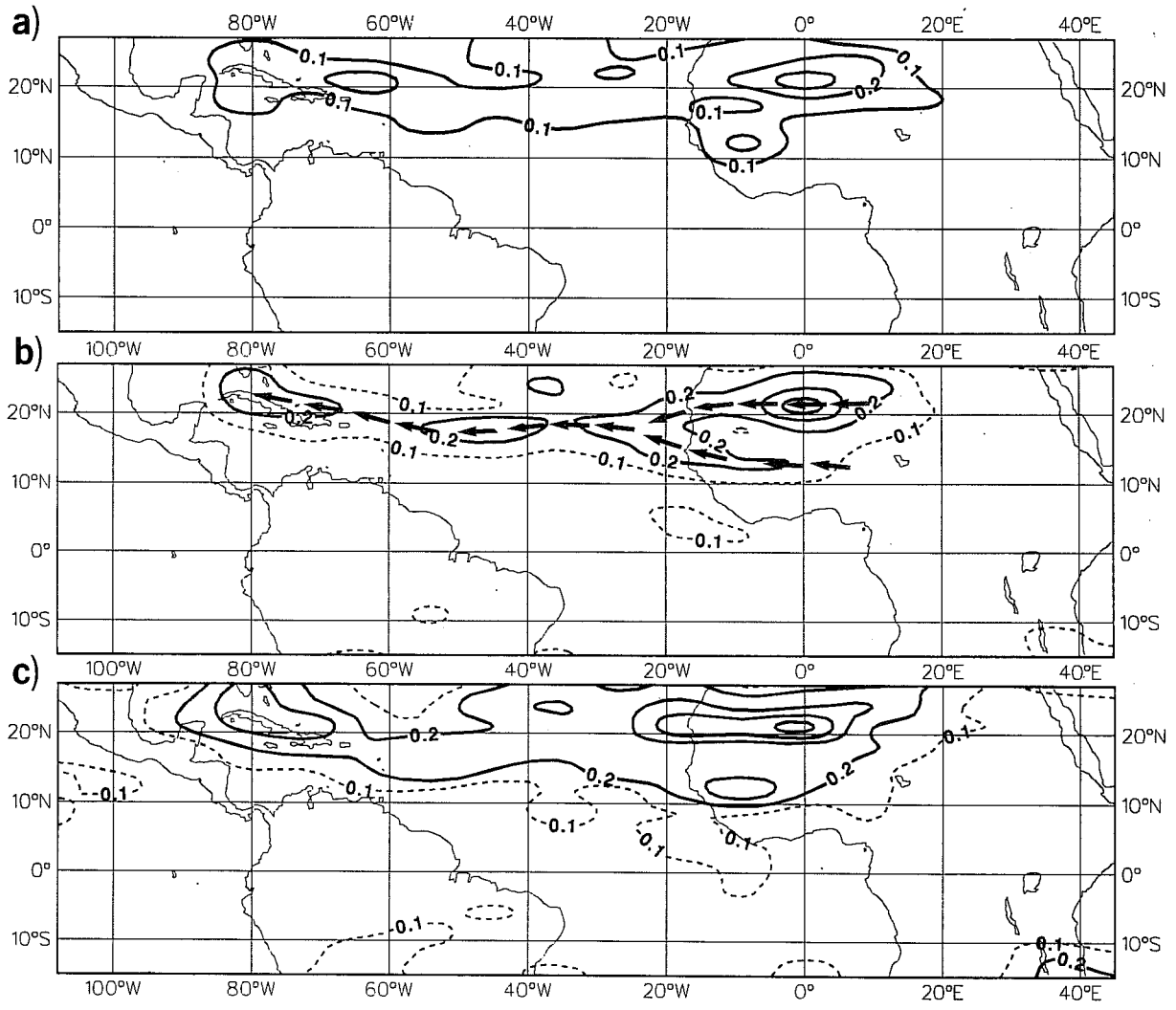

Figure 14 Variance of vorticity (10^{-10} s^{-2}) in frequency bands corresponding to periods of 2.9 to 4.0 days (a) at 850 mb, (b) at 700 mb and (c) at 700 mb for periods of 2.9 to 4.7 days. August-September, 1985. Broken arrows in (b) represent storm tracks.

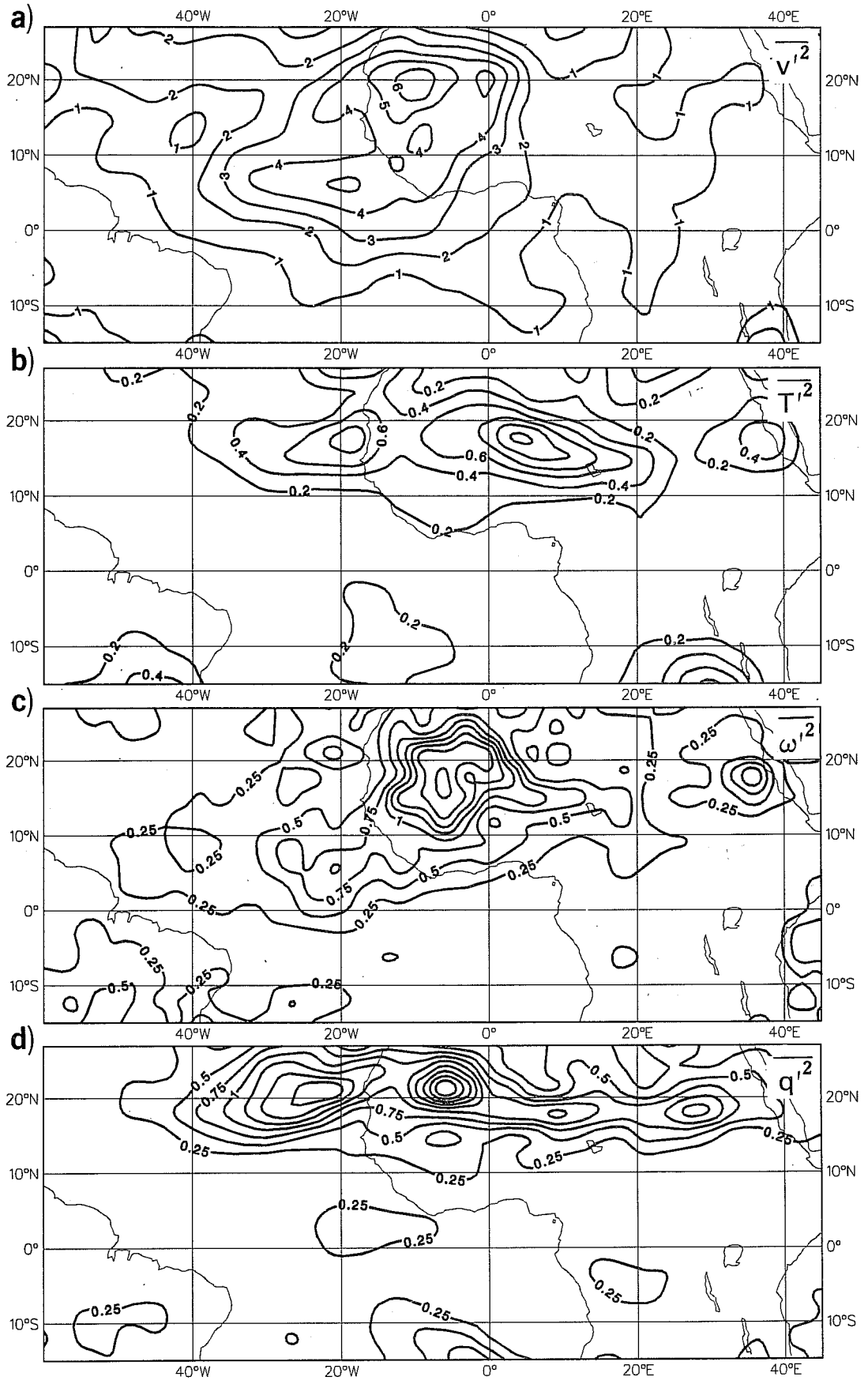

Figure 15 Variances for August-September 1985 at 850 mb for oscillations with 2.9 to 4.3 day periods of (a) meridional wind ($m^2\ s^{-2}$), (b) temperature ($[°C]^2$) and (c) vertical velocity ($10^{-3}\ Pa^2\ s^{-2}$). (d) Same for specific humidity (10^{-6}) for the 2.9 to 5.1 day period.

The variance of specific humidity (Fig. 15d) shows a zone of high value extending across Africa and the eastern Atlantic near 20°N. A number of maxima appear within the zone, the two westernmost of which are associated with aforementioned vorticity maxima.

The covariance of vertical velocity ω and temperature T at 850 mb in the 3-4 day wave band appears in Fig. 16a and the covariance for meridional wind v and temperature in Fig. 16b. The ω-T covariance has its largest magnitude in the region near 20°N, 0°, and its negative sense indicates conversion of eddy potential to eddy kinetic energy in the northern disturbances (negative omega or upward motion correlated with warm anomalies). The region of large conversion extends surprisingly far eastward near 15°N. Both the temperature variance (Fig. 15b) and omega variance (Fig. 15c) are large in the region in question, but whether there are pronounced 3-4 day peaks in the temperature and omega spectra is not known. It has already been shown that the meridional wind lacks an identifiable peak (Fig. 11).

The v-T covariance (Fig. 16b) has a maximum (negative) in the region of the ω-T maximum and additionally a stronger maximum near the coast and weaker one near 10°N, 8°W. Each of these maxima can be associated with the vorticity maximum mentioned earlier. The figure reveals that throughout West Africa and the adjacent ocean zonal available potential energy was being converted into eddy available potential energy (v and T negatively correlated in a region of northward increasing temperature). Clearly the covariance patterns are indicative of baroclinic wave development in the region near and below the AEJ. Confirmation is given to Burpee's (1972) earlier finding of a substantial negative v-T correlation at sub-Saharan stations and to his hypothesis that the baroclinity of the jet is an important factor in the wave growth.

The u-v covariance (Fig. 16c) or north-south momentum flux displays a large region of negative flux over much of West Africa. A region of positive flux that stretches westward into the central Atlantic is, however, evident south of 10°N. The pattern bears considerable resemblance to that found by Albignat and Reed (1980) for Phase III of GATE. The southward flux of westerly momentum over Africa occurs in a region of southward increase of the zonal wind component and hence indicates a growth of zonal kinetic at the expense of

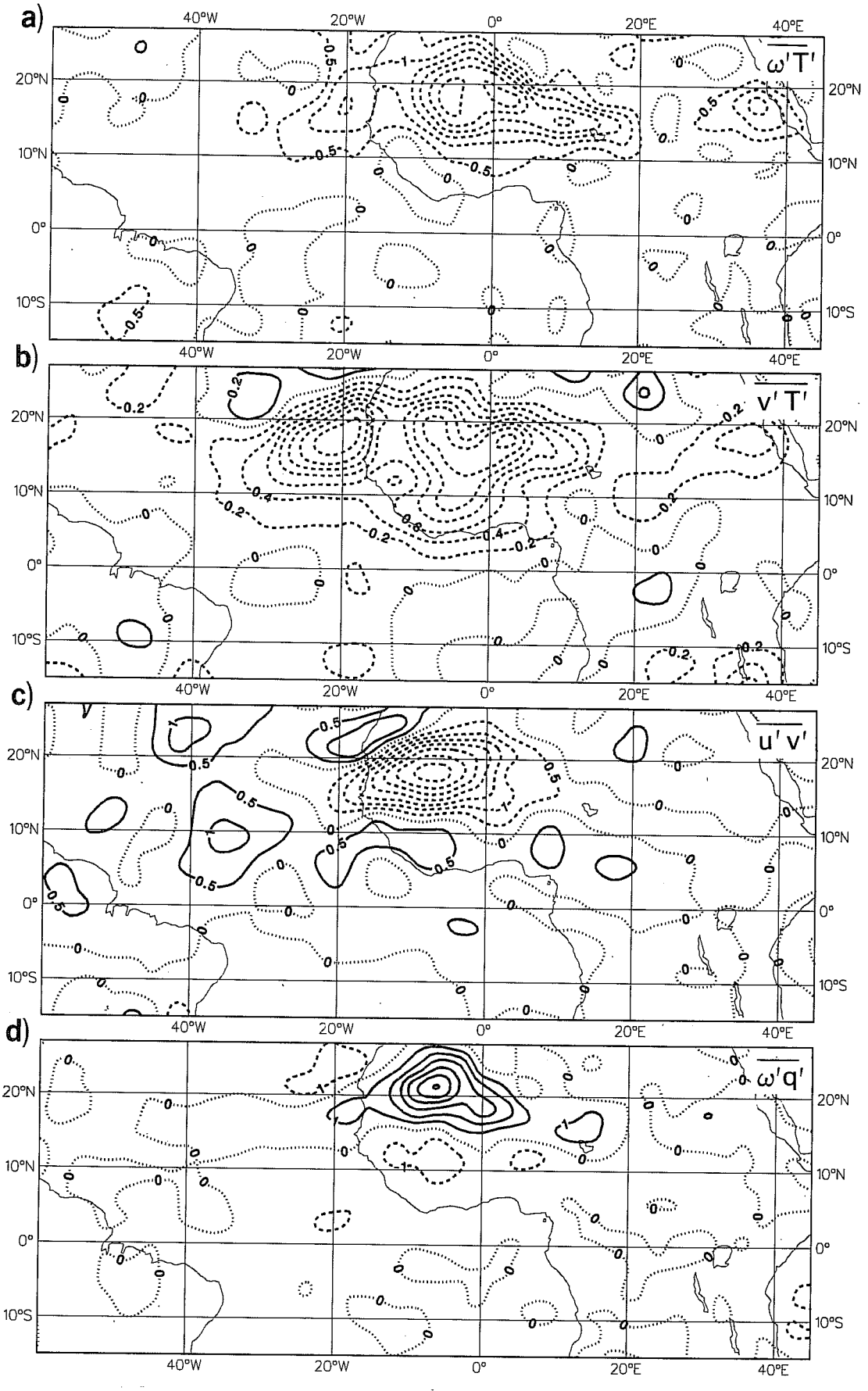

Figure 16 Covariances for August-September 1985 at 850 mb for the 2.9 to 4.3 day period for (a) vertical velocity and temperature (10^{-2} Pa s^{-1} °C), (b) meridional wind and temperature (m s^{-1} °C) and (c) zonal and meridional wind ($m^2 s^{-2}$). (d) same for vertical velocity and specific humidity (10^{-2} Pa s^{-1} g$(kg)^{-1}$) for the 2.9 to 5.1 day period.

eddy kinetic energy or a damping effect on the waves. However, the picture is quite different at 700 mb (Fig. 17) where, as in Albignat and Reed (1980), the positive and negative fluxes are properly located relative to the AEJ to convert the energy of the mean flow into wave energy. The magnitude of the fluxes are less than in Albignat and Reed and the positive maximum over West Africa is located farther to the east (see Appendix A, Fig. 10a). Burpee (1972) noted the aforementioned relationships and hypothesized that barotropic energy conversion also contributes to wave growth. The foregoing results are consistent with those obtained by Norquist et al., (1977) in their study of the energetics of the GATE waves.

The ω-q covariance (Fig. 16d) is large and positive in the region to the north of 12-15°N and negative to the south. The region of positive covariance is coincident with the region of pronounced moisture gradient (Fig. 10) and, to a somewhat lesser extent, with the region of large ω-variance. In the region of positive covariance upward motion (negative omega) is associated with negative moisture anomalies, consistent with the earlier picture of southward and upward movement of the hot (and dry) desert air in the baroclinically growing disturbances. The region of moderately large negative covariance over West Africa near 12°N lies almost directly along the axis of maximum mixing ratio. In this region upward motion is associated with positive mixing ratio anomalies, as to be expected when the horizontal moisture gradient is small and the sign of the flux is determined by the vertical gradient.

A final topic to be considered in this section is the year to year variation in wave behaviour over and in the vicinity of Africa. Interest in this topic was aroused by the considerable difference in the pattern of band-pass filtered 850 mb meridional wind variance seen in Fig. 15a and that shown in Fig. 3 of Albignat and Reed (1980), reproduced in Appendix A. Their figure revealed two maxima in 1974, one located over West Africa near 10°N and the Greenwich meridian and the second near the coast at 15°-20°N, whereas the two maxima found in this study are positioned near 20°N, 10°W and 6°N, 8°W, both regions of data deficiency. Thus questions arise concerning the reality of these maxima and the stability of the patterns from year to year. Figure 18 compares the 850 mb meridional wind variance during the August-September period for the years 1981 to 1985. Data coverage is believed to be similar in these years. Clearly year to year differences occur. In four of the five

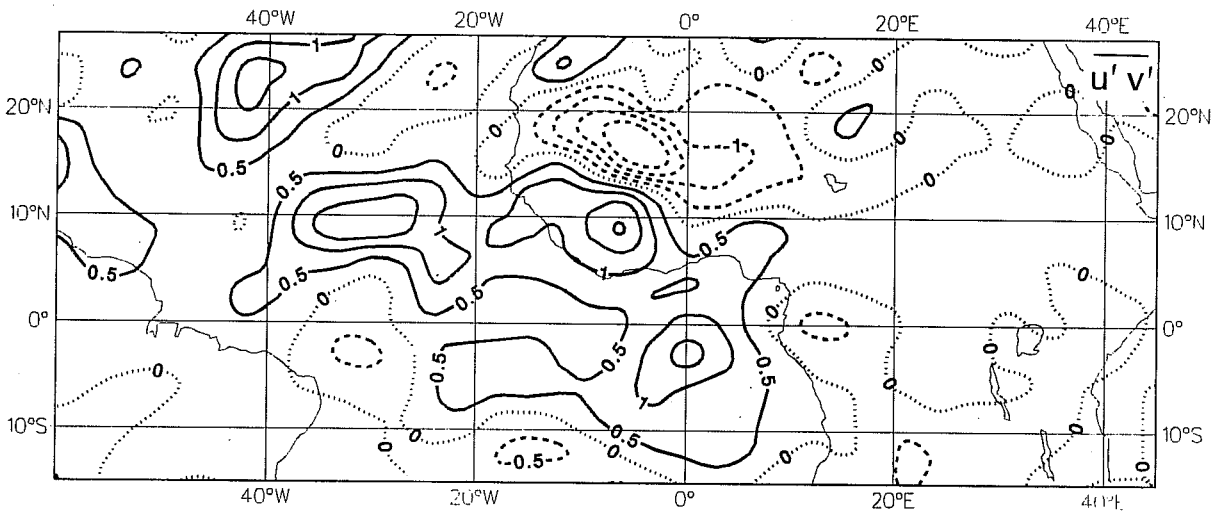

Figure 17 Covariance of zonal and meridional winds ($m^2\ s^{-2}$) at 700 mb for August-September 1985 in the 2.9 to 4.3 day wave band.

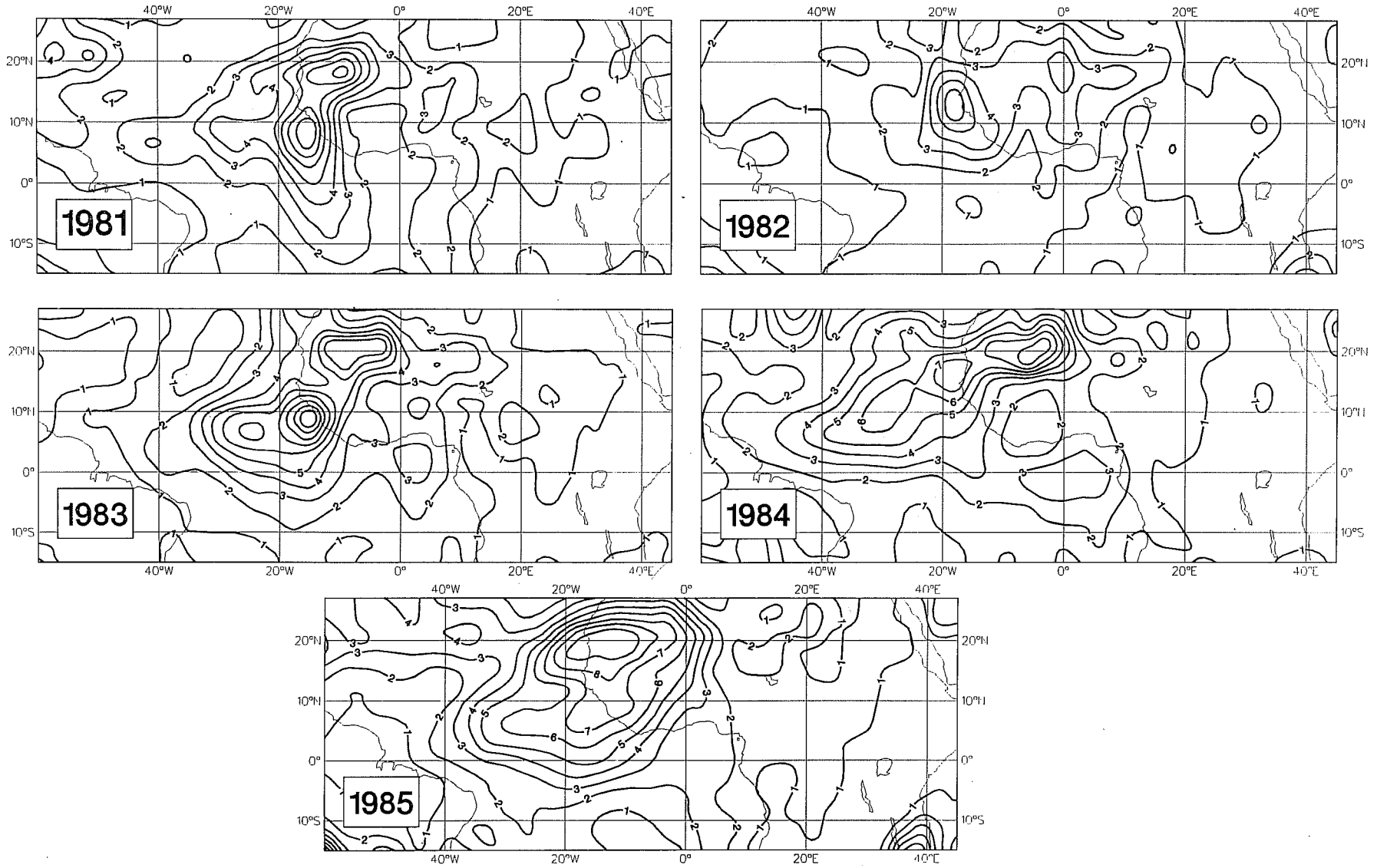

Figure 18 Variance of the meridional wind ($m^2\ s^{-2}$) for wave periods of 2.9 to 5.1 days at 850 mb for August-September of the years 1981 to 1985, inclusive.

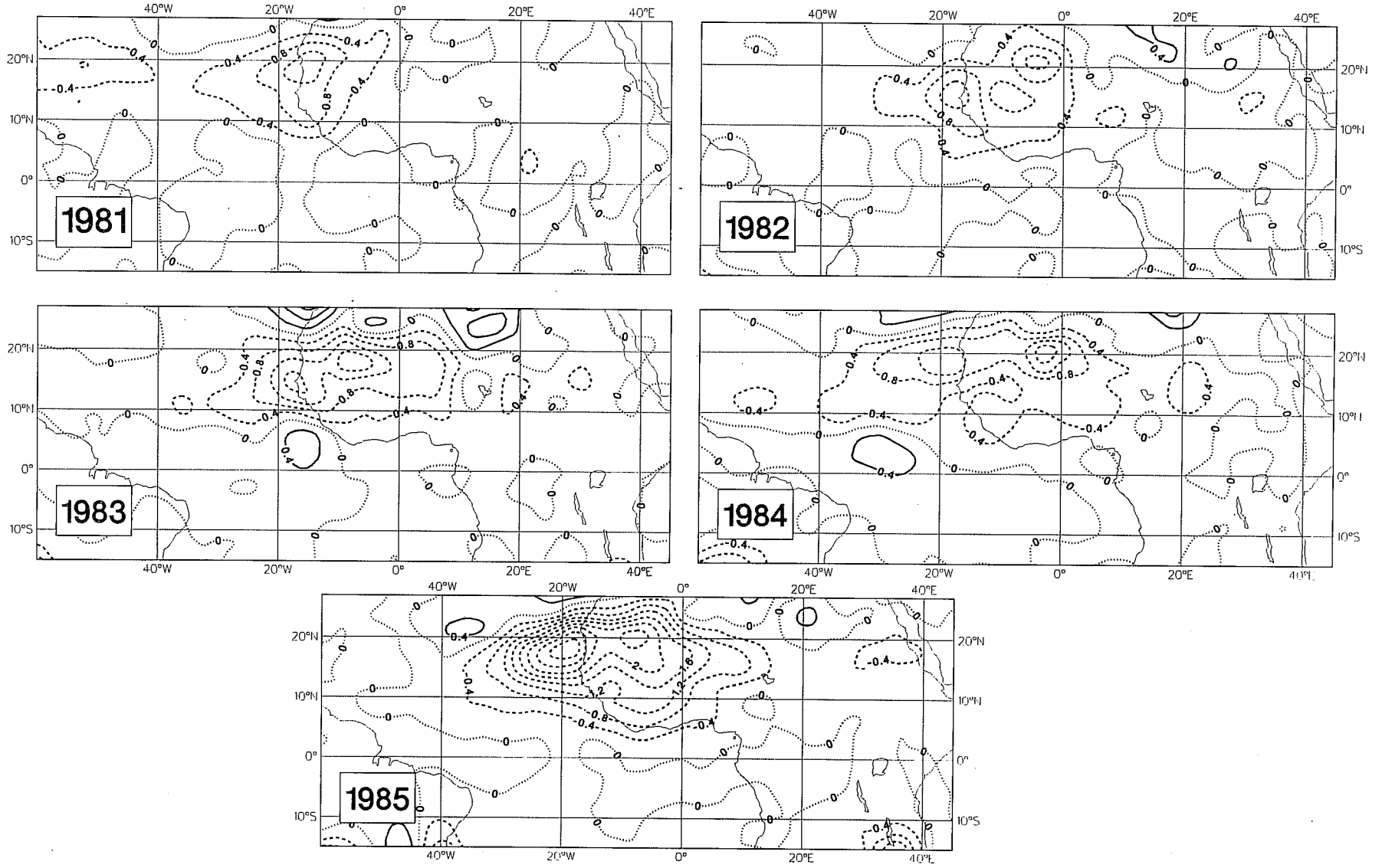

Figure 19 As in Figure 18 for the covariance of meridional wind and temperature (ms^{-1} °C) in the 2.9 to 5.1 day range.

years a prominent maximum appears near 20°N between 5° and 15°W, but in the other year, 1982, the maximum is much weaker and shifted eastward. The 1982 pattern most resembles that for 1974, though the correspondence is far from exact.

The coastal maximum is present each year but varies considerably in position. The maximum in 1984 was situated in nearly the same position as in 1974. The 1985 pattern is characterised by the most western position of the northern maximum and by the least distinct and most southerly position of the coastal maximum. As discussed in Part I, a change in model physics was made in 1985 that resulted in increased latent heat release by convection and hence better maintenance of the quasi-stationary flow. This might account in part for the southward displacement of the offshore centre to a position closer to the zone of maximum convective activity.

It is unlikely, however, that model changes can account for the differences observed in other years. We are thus led to conclude that real year to year changes take place that may account in large measure for the striking differences between the pattern observed in the GATE period and in 1985. That large differences can truly exist, especially when the time series are of short length, is illustrated by comparing Albignat and Reed's (1980) results for 1974 with Mouzna's (1984) results for 1979. In both studies the period of record was approximately a month, and data coverage was above normal as a consequence of special observing programs (GATE and FGGE). Over West Africa very remarkable differences are seen when Fig. 3 of Albignat and Reed is compared with Fig. 14a of Mouzna (see Appendix A). Near the coast, north of Dakar, the variance patterns are more alike, but Mouzna's analysis does not extend sufficiently westward for a comparison to be made in the offshore area.

The covariances of v-T or sensible heat fluxes also exhibit substantial year to year variations, as seen from Fig. 19. By far the most intense pattern occurred in 1985 following the introduction of the T106 model with revised physics. This suggests an effect arising from changes in the forecast model, but based on all evidence, we conclude, as before, that most of the year to year variation is indicative of real changes in atmospheric behaviour.

We now return to the problem of interpreting the meaning of the dual peaks that appeared in the spectra for 9°N (Fig. 12). From the bottom panel of Fig. 18, depicting the variance of the 3-5 day waves in 1985, it is seen that a region of large 850 mb meridional wind variance is centred near 8°N, 17°W and that the large values taper off quite uniformly both to the east and west. The spectra in Fig. 12 show that the variance field observed in Fig. 18 is composed of only a 3-3.5 day component east of 3°W, of mixed 3-3.5 day and 4 (or 4.5) day components between 3°W and 12°W and of only a 4 day component west of 12°W. That the combination of these spectral components leads to such a simple overall pattern may be taken as evidence that only a single phenomenon is being viewed. In support of this contention, we note that at and near 18°N the above components, seen also in Fig. 11, combine to form a smooth pattern between 12°E and 25°W whereas the combination of the 4 day wave and the 5-6 day wave - the latter already identified as a physically distinct phenomenon - leads to a more complex pattern between 30°W and 40°W.

The covariances of v-T or sensible heat fluxes also exhibit substantial year to year variations, as seen from Fig. 10. By far the most intense pattern occurred in 1985 following the introduction of the T106 model. This again suggests an effect arising from changes in the forecast model, but based on all evidence, we conclude, as before, that most of the year to year variation is indicative of real changes in atmospheric behaviour.

6. WAVE STRUCTURE

In the previous section we have used spectrum analysis to determine the basic wave parameters - wavelength, wave period and phase speed - and to map, primarily at the 850 mb level, the distributions of variances and covariances of the basic meteorological variables in the 3-4 day wave band. In this section we attempt a three-dimensional description of the wave fields, utilizing two types of representation: (1) vertical cross sections of variances and covariances taken along 9°W and (2) vertical profiles of amplitudes, phases and coherences at selected points along 18°W. The 18°W meridian was selected because it passed through the regions of large wave variance associated with the tracks of both northerly and southerly disturbances (Fig. 15a) and because it was situated close to the longitude (23.5°W) of the centre of the GATE B-scale ship network. An unusually detailed knowledge of the wave structure has been obtained for that area (Thompson et al., 1979).

6.1 Vertical cross sections of variances and covariances

The distributions of the variances are shown in Figs. 20a-d. A main feature of the cross section depicting the meridional wind variance (Fig. 20a) is the region of large variance situated at 20°N and 850 mb. This region tilts southward with height so that at 700 mb it is located near 15°N. A secondary maximum at 15°N and 200 mb is believed to be a manifestation of the deeper wave structure that exists at latitudes where organized convection occurs (Reed et al., 1977). The large variances near the equator at 500 mb and 200 mb were not observed during GATE and need further investigation. Inspection of synoptic maps at 200 mb suggests that the near-equatorial fluctuations are associated with variations in the Tropical Easterly Jet. The variations seem to be of two types - variations in the speed of the jet, where the variations originate over Central Africa or further east, and variations in the strength of the north-easterly monsoonal component of the outflow from West Africa to the southern hemisphere. The analysed variations at 200 mb are supported by aircraft or cloud track wind data over the Gulf of Guinea when such data are available. The coherence between the wave spectra in the easterly wave region and the spectra in the Tropical Easterly Jet region is low, which rules out a close connection between the two phenomena.

The geopotential height variance (Fig. 20b) presents a simple picture. The wave amplitude is largest near 20°N and diminishes with height. The upper-level variance maximum near 30°N is undoubtedly associated with middle latitude systems, not tropical waves. The cross section of temperature variance (Fig. 20c) shows that the maximum thermal variation occurs at 850 mb slightly to the south of 20°N. A weaker maximum that may be associated with latent heat release is visible near 15°N and 400 mb. Other thermal features are believed to be unrelated to the waves.

The variance of vertical motion (Fig. 20d) is particularly interesting. Strong fluctuations occur at low levels between 15°N and 20°N. The region of large variance extends upward and southward, and a secondary maximum appears just south of 10°N. The pattern is reminiscent of the patterns of mean vertical motion along 20°E and, to a lesser degree, along 0°. (Figs. 6d and c). Again the dichotomy between shallow wave structure in the monsoon trough to the north and deeper structure in the rain belt to the south is seen.

Covariance patterns are shown in Figs. 21a-c. The regions of large negative covariances of ω-T and v-T seen previously near 20°N on the 850 mb charts (indicative of regions of conversions from eddy available potential to eddy kinetic energy and of zonal to eddy available potential energy, respectively) are shown to be relatively shallow features that extend only to the middle troposphere (Figs. 21a and b). A secondary region of large v-T covariance near 10°N, noted earlier, is also seen to be a shallow feature. Between the equator and 10°N there exists a deeper but weaker region of positive ω-T covariance signifying an opposite energy transformation (Fig. 21a). Above, near 300 mb, there is a small region, coincident with the upper region of large ω-variance in Fig. 20d, in which the conversion is again negative, i.e. from eddy available potential energy to eddy kinetic energy.

The u-v covariance or momentum flux (Fig. 21c) shows the aforementioned region of negative covariance at 20°N to be confined mainly to the lower levels. A deep layer of positive covariance appears at middle levels further to the south. This region, which lies on the cyclonic side of the AEJ, is associated with the conversion of zonal kinetic to eddy kinetic energy and is the basis of the idea, first proposed by Burpee (1972), that barotropic instability plays a part in African wave development. A large divergence of momentum flux

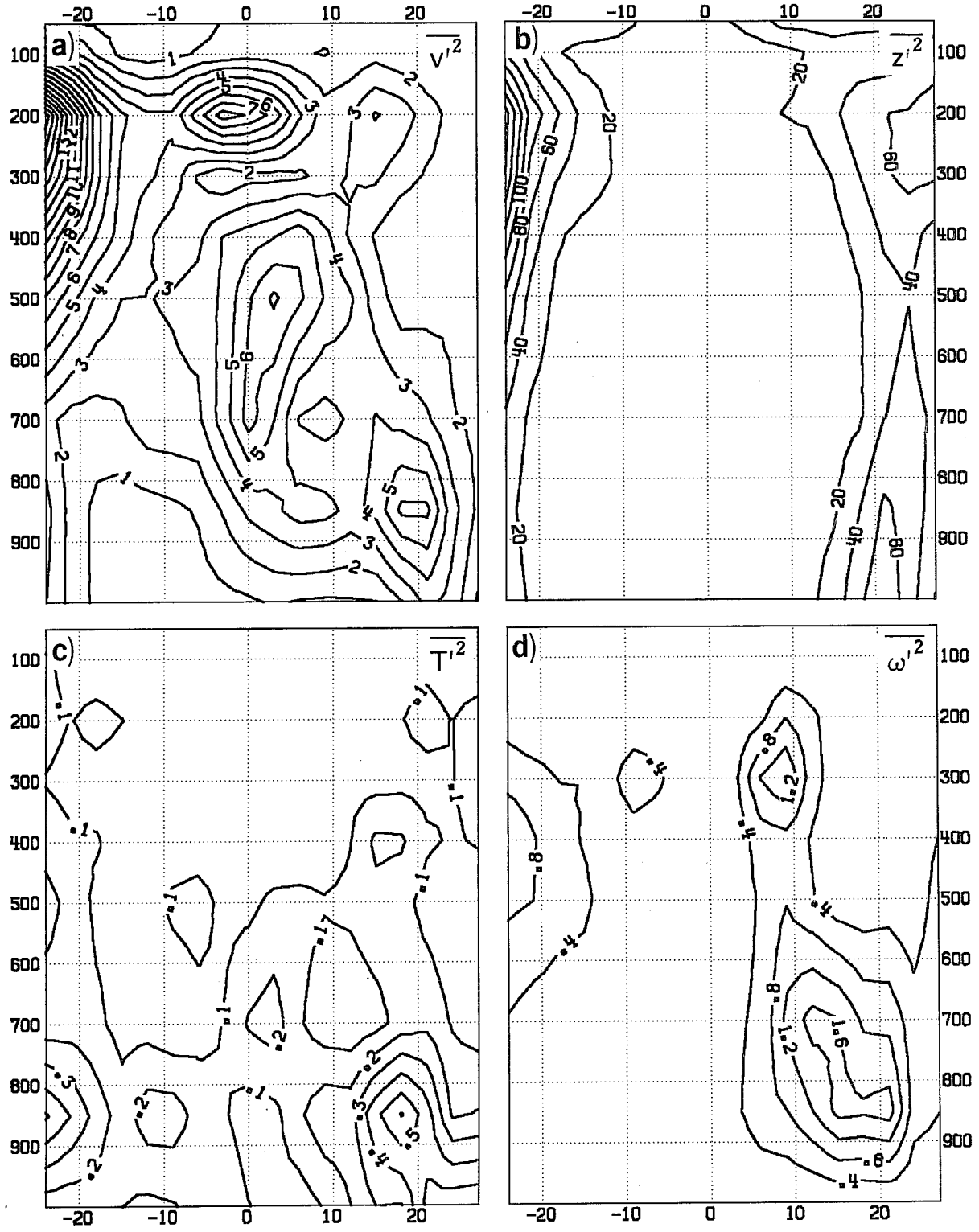

Figure 20 Meridional sections along 9°W for August-September 1985 of variances of (a) meridional wind ($m^2\ s^{-2}$), (b) geopotential height (m^2), (c) temperature ($[°C]^2$) and (d) vertical velocity ($10^{-3}\ Pa^2\ s^{-2}$) for waves of 2.9 to 4.3 day periods.

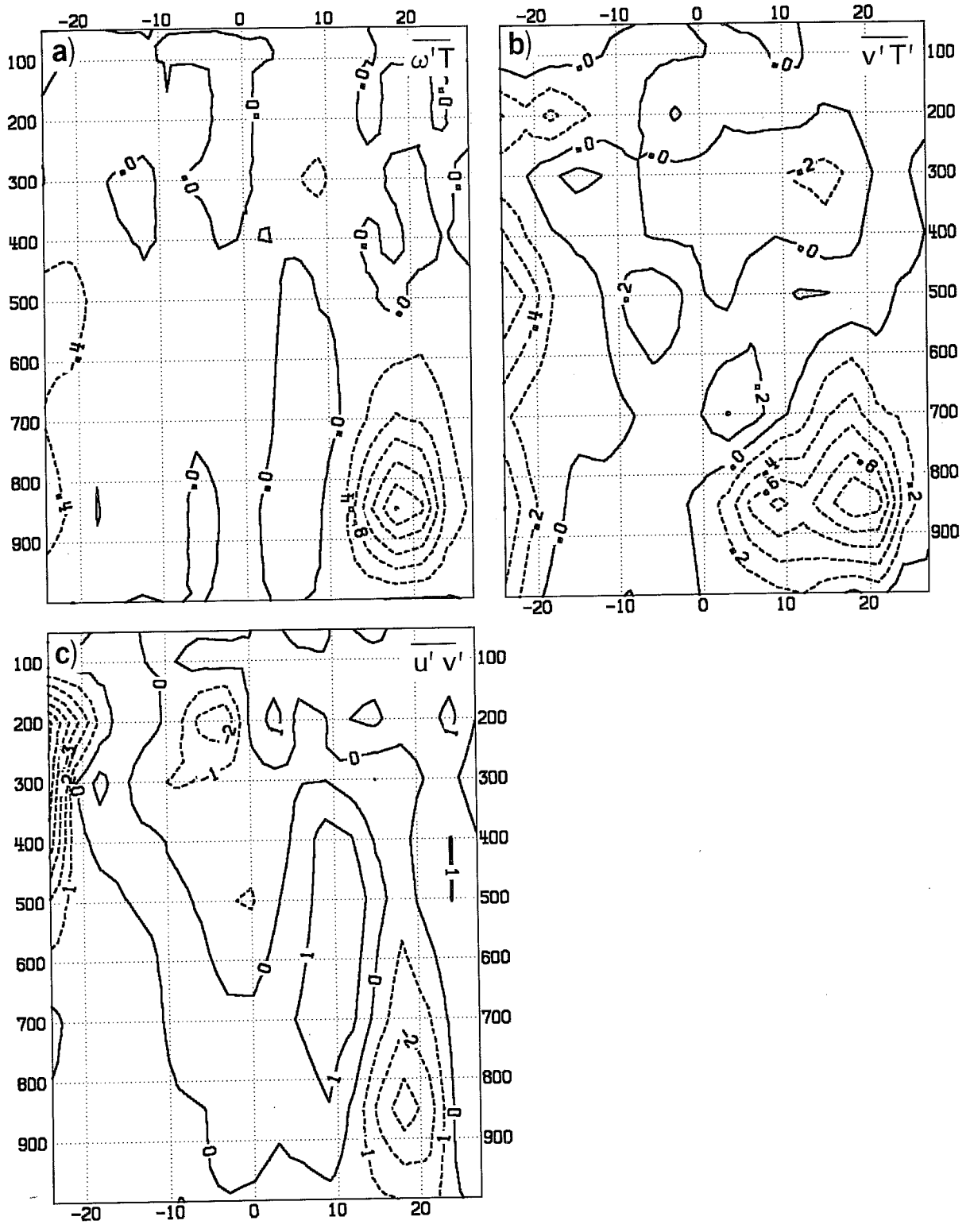

Figure 21 As in Figure 20 for covariances of (a) vertical velocity and temperature (10^{-2} Pas^{-1} °C), (b) meridional wind and temperature (ms^{-1} °C) and (c) zonal and meridional wind (m^2 s^{-2}).

occurs in the vicinity of the equator at 200 mb. This is the region where a pronounced unexplained maximum in the variance of the meridional wind component exists (Fig. 20a). The origin of the flux divergence also requires explanation.

6.2 Vertical profiles of amplitudes and phases

We consider now the amplitude and phase variations at 18°W. Amplitudes, normalised with respect to the maximum value of the particular variable measured in the column, appear on the top left hand side of Figs. 22a, b, c, phases appear at the bottom, and coherences appear at the top right hand side. To show phase relationships it is necessary to choose a reference parameter and reference level. We have chosen for this purpose the meridional wind component at 850 mb. All other phases are displayed relative to it, and the coherences pertain to these phase calculations. Larger coherences are presumed to be indicative of significant phase relationships, but we have not attempted to assess precise significance levels. The presentation is such that a positive phase difference signifies that the phase of a particular variable lags that of the 850 mb meridional wind. Since the waves propagate westward, a positive phase tilt with height signifies, for instance, an eastward tilt in space. For purposes of comparison with synoptic studies of wave structure it is convenient to regard the phase diagram as an east (right) to west (left) cross section. Inasmuch as amplitude variations with height have already been discussed for a nearby longitude, the discussion here will concentrate on the phase diagrams.

The following coherent structures appear on the phase diagram for 21°N, 18°W (Fig. 22a).

(1) Between the surface and 400 mb the maximum south wind lies a quarter cycle ahead of (west of) the maximum geopotential height of ridge, as to be expected from the geostrophic relationship. Both fields tilt eastward with height at lower and middle levels. The tilt reverses above 400 mb where the coherence is small.

(2) Below 700 mb warmest temperatures are roughly 180° out of phase with the south wind maximum, indicating, as previously, a correspondence between northerly winds and positive temperature anomalies. This relationship results, of course, from the presence of the hot desert to

the north. Above the level of the desert heating (600-500 mb), where the north-south thermal gradient reverses sign (Fig. 9b), an opposite relationship holds.

(3) As found previously, at the levels of largest coherence between v and ω (850 mb and 700 mb) sinking motion (positive ω) is associated with southerly winds, or, to put it oppositely, ascent occurs in the hot desert air advected southward ahead of the trough.

(4) The only other coherent relationship noted is the association below 850 mb of westerly winds with the ridge and above 400 mb with the trough (at 850 mb). A slight positive momentum flux is observed at 850 mb.

The picture at 15°N, 18°W (Fig. 22b) has a number of features in common with that at 21°N. The meridional wind maximum and pressure ridge tilt eastward with height in agreement with the association of cooler temperatures with southerly winds. Rising motion at 850 mb occurs in conjunction with northerly winds and positive temperature anomalies. However, a shift to a slight negative momentum flux occurs at 850 mb, and new features of significance appear at higher levels (400-200 mb), where the meridional wind component, temperature and vertical motion all show moderate coherence with the 850 mb wind. The wind maximum at these higher levels tilts westward with height, and the temperature at the level of maximum coherence (300 mb) is positively correlated with southerly winds at the lower (and the upper) level. The vertical motion (ω) at 300 mb is out of phase with the southerlies and with the warm temperatures aloft (signifying rising warm air or negative ω-T covariance). The latter relationship is barely evident at 15°N in the ω-T covariance section for 9°W (Fig. 21a), where it appears to be connected with the region of negative covariance centred at 8°N. We regard the feature in question to be a manifestation of the effect of convection in producing deep wave structure. This interpretation is borne out by the continued association of warm anomalies with rising motion at levels near 300 mb in the convectively active region near 9°N (Fig. 22c) and by the association there, above 100 mb, of cool anomalies with rising motion. These convective signatures have been noted previously (Reed et al., 1977; Thompson et al, 1979).

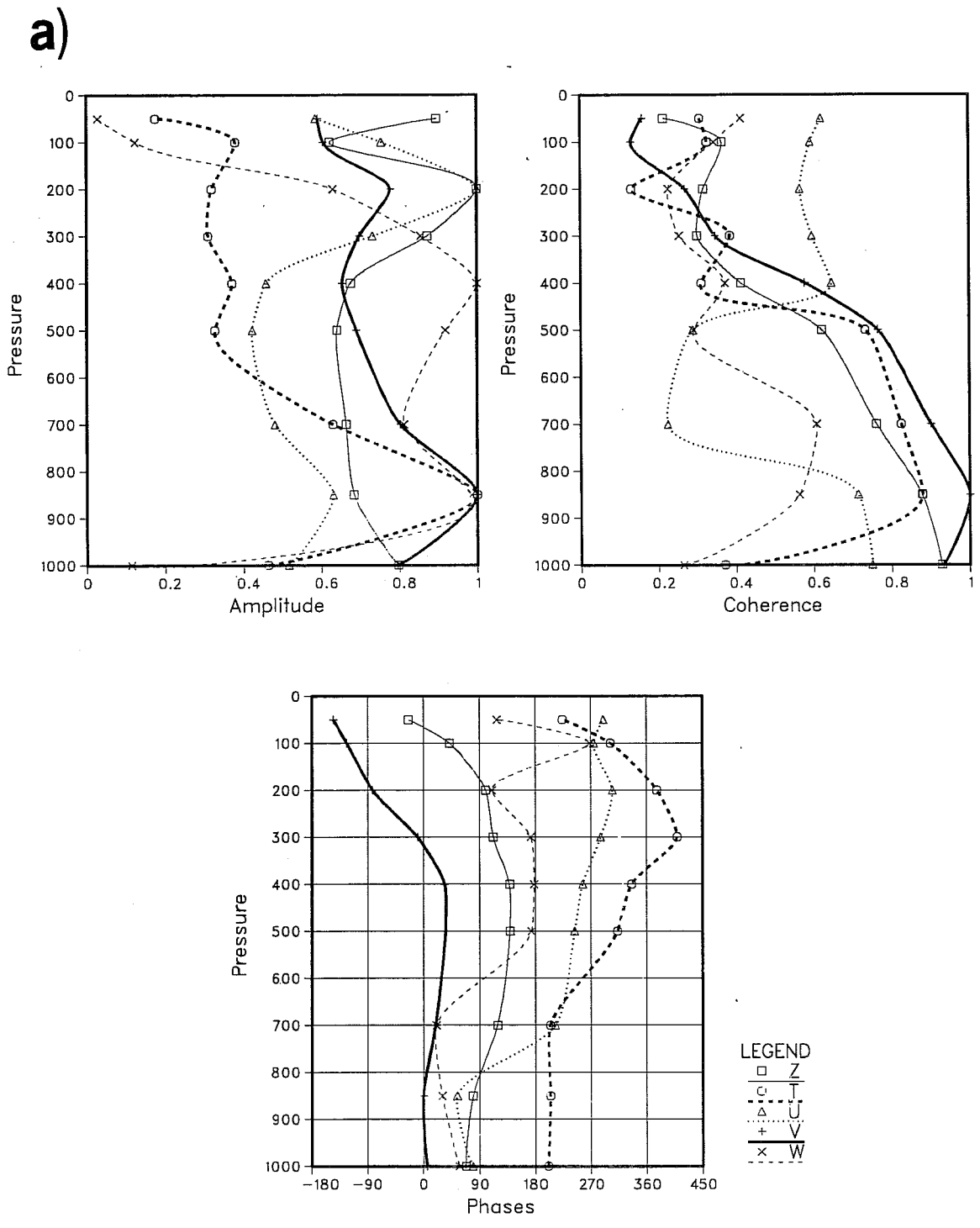

Figure 22 (a) Vertical profiles at 21°N, 18°W, for August-September, 1985, and for 2.9 to 5.1 day periods, of normalized amplitude (top left), coherence (top right), and phase (bottom). See text for further explanation.

b)

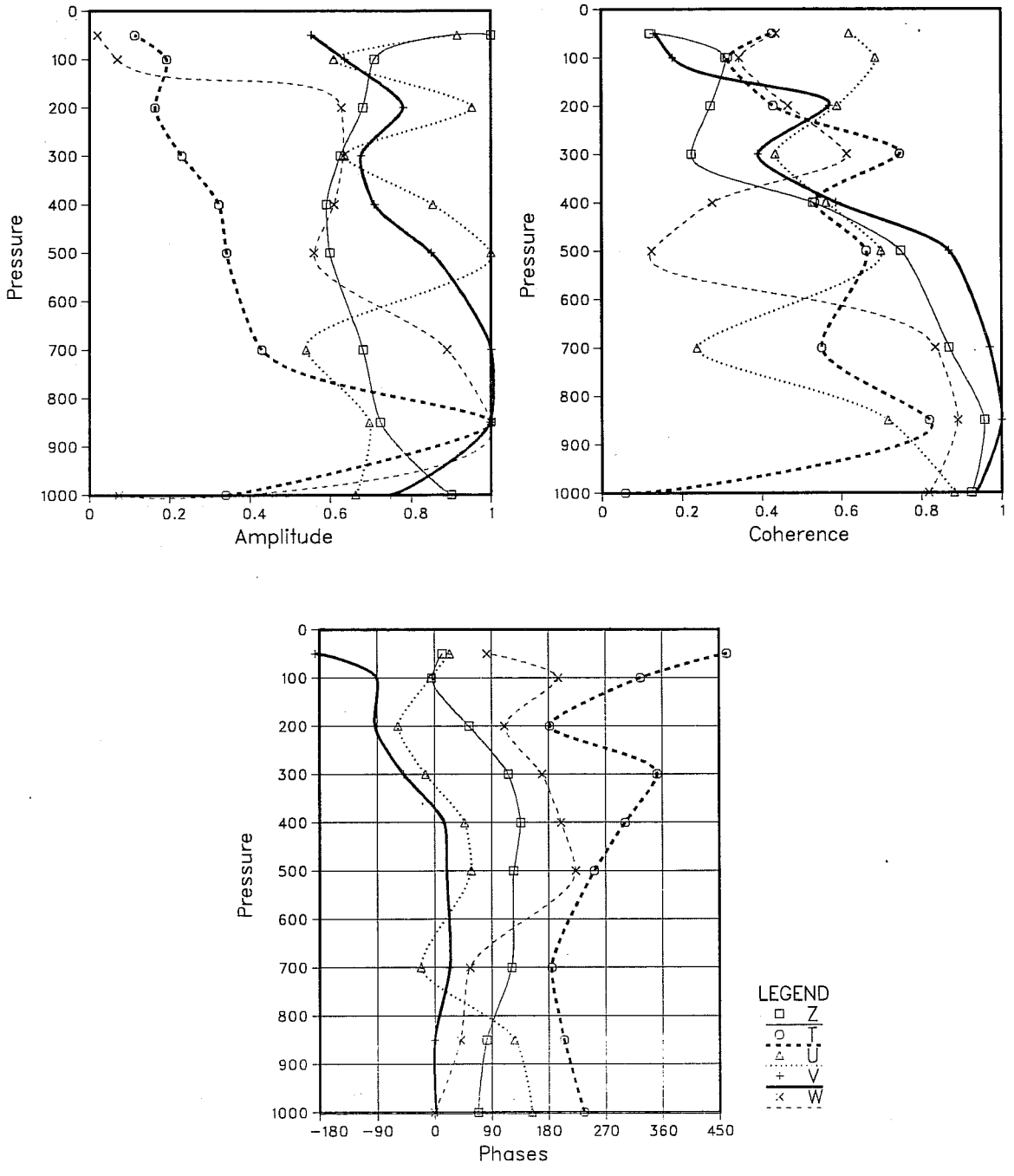

Figure 22 (b) As Fig. 22a for 15°N, 18°W.

c)

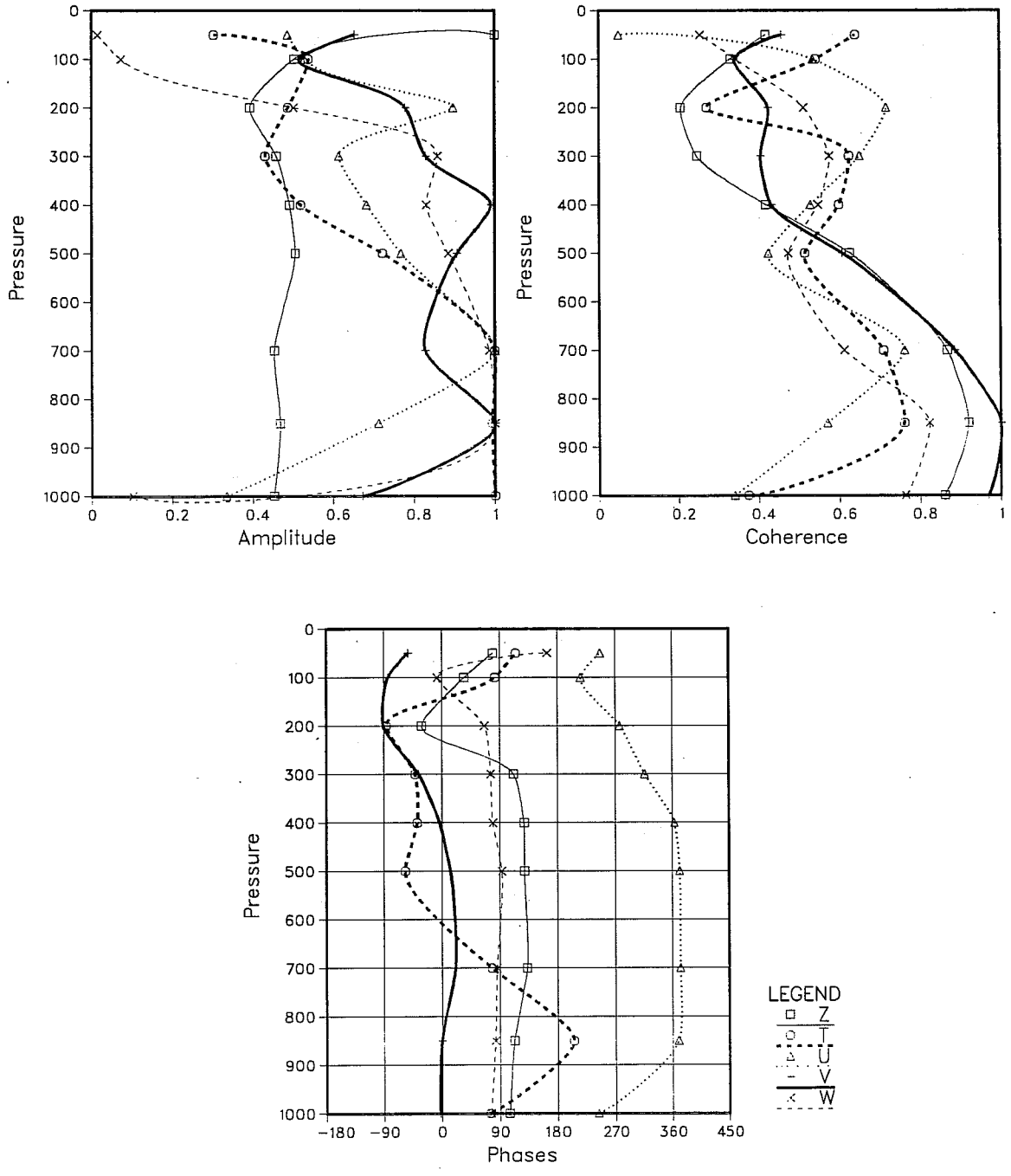

Figure 22 (c) As Fig. 22a for 9°N, 18°W.

A further feature of interest on the diagram for 9°N (Fig. 22c) is the association of southerly winds with westerly winds at levels between 700 mb and 400 mb where amplitudes are sizeable and coherences large. This shows again the existence of positive momentum flux and barotropic wave growth to the south of the AEJ. A final feature to be noted is the weakening of the association of southerly (northerly) winds and cool (warm) temperature in the lower atmosphere as one moves southward from the Sahara (except at 850 mb itself) and a weakening of the association of sinking (rising) motion with southerly (northerly) winds.

6.3 Comparison of wave structure during August-September 1985 with that during Phase III of GATE

A detailed summary of the wave structure observed during Phase III of GATE and a discussion of the origin and maintenance of the waves based on the observed structure can be found in Reed (1979). Papers that contributed to the description and that are of particular interest here are Reed et al., (1977) and Norquist et al., (1977). A later paper by Albignat and Reed (1980) is also pertinent to the discussion. In order to make the comparison as succinct and meaningful as possible, we first review the basic ideas on wave dynamics that have emerged from these and other studies and then single out for comparison those structural features seen in the GATE analyses that are particularly relevant to the wave dynamics. Prominent structural features seen in the August-September 1985 data but not observed in the GATE data are also of concern. These features, few in number, will be mentioned at the end of the section.

The picture of the wave dynamics that emerged from the GATE analysis in that of a two component system: one a baroclinically and barotropically driven component connected with the instability of the AEJ and a second convectively driven component possibly connected with wave-CISK (Lindzen, 1974). Burpee (1972) was the first to demonstrate the importance of the AEJ to wave development; Carlson (1969) pointed out the possible importance of convective activity. Carlson also remarked on the tendency of African waves to possess two centres at the surface: a relatively cloud-free centre situated along the southern fringe of the Sahara and a weaker centre further south characterized by larger cloud amounts and presumably more convective activity. The dual centres were also identified in the GATE analyses of Burpee (1975) and Reed et al., (1977).

In the GATE studies the northern component of the system had the hallmarks of a moderately shallow, baroclinically-growing disturbance. In the region between about 12°N and 20°N and below the core of the AEJ, where easterly shear existed in the vertical, warm (dry) air flowed southward and upward, cool (moist) air flowed northward and downward, and the wave axis tilted eastward (opposite to the shear) with height (Reed et al., 1977). Wave energetics computed for this region showed pronounced conversions from zonal to eddy available potential energy and from eddy available potential energy to eddy kinetic energy (Norquist et al., (1977).

The southern component of the system possessed a deeper and quite different structure. The thermal field was marked by a three-tiered structure, suggesting a substantial effect by convective processes (Reed et al., 1977). In the lower atmosphere cool anomalies were found in the wave trough where rainfall was abundant and thus where evaporative cooling or cooling by downdrafts was expected to be abnormally large. At middle and upper levels, on the contrary, warm anomalies appeared. These presumably were caused by latent heat release in convection. At still higher levels, near the tropopause, cool anomalies reappeared. These have been attributed to the cooling produced by overshooting cumulus towers, Reed (1979).

The vertical velocity pattern in the southerly part of the wave system displayed a middle to upper level maximum that was distinct from the maximum observed lower down and to the north. The maximum upward motion was associated with the aforementioned middle to upper level warm anomaly (Reed et al., 1977). The conversion of eddy available potential energy to eddy kinetic energy in the warm layer well exceeded the opposite conversions in the layers above and below, yielding a net contribution to wave growth within the near equatorial rain belt. (Norquist et al., 1977). In this region, unlike further north, the waves exhibited no pronounced tilt with height (Albignat and Reed, 1980).

The role of barotropic instability in wave development requires further clarification. Burpee (1972) in his observational study found that the vertical (baroclinic) and lateral (barotropic) shears of the AEJ contributed almost equally to wave generation. Numerical modelling studies have indicated an even greater importance of barotropic instability in supplying the kinetic energy of the disturbances (Rennick, 1976; Simmons, 1978; Mass, 1979).

However, the simple picture of a major or primary role for barotropic instability in wave initiation is complicated by the finding of Norquist et al., (1977). They found that the barotropic energy conversion during Phase III of GATE was much stronger over the eastern Atlantic, where the waves had already achieved peak strength and were on the verge of a rapid decline, than over Africa, where they experienced their initial and major growth. This behaviour is strikingly apparent in Figs. 7 and 10a (see Appendix A) of Albignat and Reed (1980). The increase in amplitude of the meridional wind component at 700 mb (and 850 mb) takes place between 15°E and the prime meridian. The barotropic energy conversion in this region, as judged from the 700 mb momentum flux, is small and barely positive. On the other hand, the barotropic conversion is very large in the offshore region near 10°N, 20°W. From Thompson et al., (1979) it is also known to have been large within the GATE B-scale ship network even farther to the west. Thus it seemed possible from the GATE results that the role of barotropic energy conversion may be more to preserve the waves as they enter and adjust to a different large-scale environment than to generate them initially.

We turn now to Table 1 which lists the main baroclinic, barotropic and convective structural features evident in the GATE data and which compares the findings of the present investigators (referred to as RKH) concerning these features with the results of Reed et al., (1977), Norquist et al., (1977) and Albignat and Reed (1980), hereafter referred to as RNR, NRR and AR, respectively. Pertinent figures in the text are noted. Those from the GATE papers are also noted in the table and are reproduced in Appendices A, B and C. The structural features in question are listed in the left hand column of Table 1. Their characteristics in the GATE analyses are noted in the middle column. The characteristics of the same features in the August-September 1985 analyses, if observed, are noted in the right hand column. It must be kept in mind that exact comparison is not possible, since the GATE description is based mainly on a composite wave structure representative of the region from 30°W to 10°E while the August-September 1985 description is spectral in character and focuses largely on cross sections along 9°W and 18°W.

From Table 1 it is apparent that the baroclinic features seen during Phase III of GATE were almost exactly repeated during August-September 1985. The latitude of maximum baroclinic energy conversion, as represented by the

position of maximum $\overline{v'T'}$ and $\overline{\omega'T'}$, was slightly further north in 1985 and the eastward tilt of the wave axis with height extended farther to the south, but all essential features are the same.

Similarly, the barotropic features were much the same in the two periods. However, from Fig. 17 (taken in conjunction with Figs. 4b and c) it is apparent that the maximum barotropic energy conversion in the August-September 1985 period occurred in the region from 5° to 10°W, well to the east of the region of maximum conversion during the GATE period (see Fig. 10a, Appendix A). This suggests a more important role for barotropic instability in the initial wave development during the August-September 1985 period.

The convective features, too, show a remarkable correspondence between the two periods. Some minor discrepancies, however, are noted. The cold anomaly present in the wave trough between the surface and 700 mb at 12°N in 1974 does not appear at 850 mb and 12°N in 1985, though it does appear above and below. Instead the colder temperatures at this level lie to the rear of the trough as in the dry baroclinic disturbances to the north, and the wave axis continues to tilt eastward with height rather than to be vertical, as in 1974. Another discrepancy is the absence of a pronounced region of positive ω-T covariance at high levels, a feature clearly evident in 1974.

Finally, we call attention to certain features in the present analyses that were not seen in the GATE data. First, are the large variances of the meridional wind component near the equator at 500 mb and 200 mb (Fig. 20a) and associated with these variances, particularly at 200 mb, the large divergence of momentum flux (Fig. 21c). We are unaware of such features being observed at wind measuring ships that were stationed near and on the equator during GATE. These features may be spurious but as noted earlier they have some support from Aircraft and cloud track wind data over the Gulf of Guinea; their nature is not understood. A second item of note is the secondary maximum of southward heat flux (negative $\overline{v'T'}$) that appears at 850 mb and 9°N in Fig. 21b. No trace of such a feature is found in RNR. A third feature is the region of negative $\overline{v'T'}$ that appears in the same figure at 300 mb and 10°-15°N. This too has no counterpart in RNR.

Table 1 Comparison of Wave Structure during August-September 1985 with Structure during Phase III of GATE. The cited figures by AR, RNR and NRR are reproduced in Appendices A, B and C, respectively.

Baroclinic Features	1974	1985
Warm T, northerly v	850 mb, 15°-20°N RNR: Figs. 4b, 7c	900-700 mb, 12°-21°N RKH: Figs. 22a-c
Warm T, upward ω	850 mb, 15°-20°N RNR: Figs. 7a and c	700-900 mb, 15°-21°N RKH: Figs. 22a and b
$\overline{v'T'}$, negative max in region of $\partial\overline{T}/\partial y>0$	850 mb, 16°N NRR: Fig. 4	850 mb, 18°N RKH: Fig. 21b
$\overline{\omega'T'}$, negative max	850 mb, 16°N NRR: Fig. 3	850 mb, 18°N RKH: Fig. 21a
Eastward tilt of wave axis with height	North of 12°N 0-45° phase tilt, 850-700 mb AR: Fig. 12	12°-21°N 20-30° phase tilt, 850-700 mb RHK: Figs. 22a-c
Barotropic Features		
v southerly, u westerly	12°N, 850-100 mb RNR: Figs. 8a and b	12°N, 850-200 mb RKH: Fig. 22c
$\overline{u'v'}$, maximum in region of negative $\partial\overline{u}/\partial z$	11°N, 650 mb; NRR, Fig. 2 9-13°N, 700mb; AR: Fig. 7	11°N, 550 mb RKH: Fig. 22c
Convective Features		
Cold trough at lower levels	12°N, 1000-700 mb RNR: Fig. 9b	12°N, only near 900 mb and 700 mb; RKH: Fig 22c
Middle and upper level warmth in and to east of trough	12°N, 600-250 mb RNR: Fig. 9b	12°N, 500-250 mb RKH: Fig. 22c
High-level cold in trough region	12°N, 200-100 mb RNR: Fig. 9b	12°N, 100-50 mb RKH: Fig. 22c
Distinct upper-level max in ω amplitude or variance	300 mb; RNR: Fig. 11a 8°N; RNR: Fig. 7b	300 mb, 9°N RKH: Fig. 20d
Warm T, upward ω	0°-15°N, 300 mb. RNR: Figs. 7b and d	12-18°N, 300 mb RKH: Figs. 22b and c
$\overline{\omega'T'}$, positive max $\overline{\omega'T'}$, negative max $\overline{\omega'T'}$, positive max	750 mb, 9-10°N 300 mb, 10-11°N 150 mb, 10-11°N NRR: Fig. 3	700 mb, 6°N 300 mb, 9°N Not present RKH: Fig. 21a
No tilt of trough axis with height, 850-700 mb	South of 12°N AR: Fig. 12	Tilt remains

In view of the evidence presented earlier of substantial differences between the locations of the regions of maximum wave activity in Phase III of GATE and in August-September, 1985, it would be unwise to attribute the rather minor structural differences noted in the table and in the second and third items immediately above to shortcomings of the operational analysis/forecast system. Nevertheless, there is a need to explore further whether they could have been caused at least in part by slight deficiencies in the convective parameterization scheme or other aspects of the model physics. The possibly spurious features noted in the first item above clearly need further investigation.

7. FORECAST PERFORMANCE

Two aspects of the forecast performance are considered: firstly, the phase difference in the 3-5 day wave band between the analysed and corresponding 48h forecast time series of 850 mb meridional wind at points along 18°N and, secondly, for the same wave band and level, the change of variance and covariance fields with forecast interval for a number of meteorological parameters. From the phase differences between analysed winds and forecast winds for corresponding times, systematic errors in the zonal displacements of the 3-5 day waves can be determined and compared with the systematic errors found in the companion synoptic study. Comparison of the forecasted variance fields with the analysed fields provides an indication of how well the wave intensities, and the spatial distributions of the intensities, were preserved during the forecast interval. Comparison of covariance fields provides information regarding the preservation of phase relationships. Obviously, for a set of perfect forecasts, analysed and predicted variance fields should be the same, as should analysed and predicted covariance fields. One should therefore bear in mind that the spectral variances in the forecast ensembles may have a contribution from random forecast errors (Klinker and Capaldo, 1986).

7.1 Systematic errors in 48h forecasts of wave displacement

Phase differences between time series of analysed 850 mb winds and of corresponding winds from 48 h forecasts are shown in Fig. 23 for points along 18°N at 3 degree intervals between 3°W and 60°W. Also shown are the coherences between the analysed and forecast time series. The coherences are generally in the range 0.8 to 0.85, indicative of high correlation between the observed and forecast wind oscillations. Smoothed phase differences vary from zero near the eastern extremity to approximately -20° near the western. The -20° phase difference means that the forecast waves lag approximately 5h (20/360 or one-eighteenth of a 3-5 day cycle) behind the analysed waves after a lapse of two days. Equivalently, with use of the previously found 2700 km wave length, it means that the forecast waves were systematically displaced roughly 150 km or 1.4 degrees of longitude to the east of the analysed waves. In the same range of longitudes, the synoptic investigation (Table 2 of Part I) yielded position errors that varied between 0.6° long and 1.5° long. The errors were in the sense indicated by the spectral results, i.e. the forecasted positions tended to be to the east of the analysed (or observed)

positions. Thus both synoptic and spectral investigations reveal that over West Africa and the central and eastern Atlantic the waves tended to travel westward at a somewhat faster speed than given by the forecasts.

7.2 Comparison of analysed and forecast variance and covariance fields

Figure 24 shows maps of the 850 mb meridional wind variance during August-September, 1985, for the analysed winds (Fig. 24a), for the 48 h forecast winds (Fig. 24b) and for the 72h forecast winds (Fig. 24c). The most striking feature of the maps is the overall decline in wave intensity during the three day period. Another feature of interest is the migration of the centre of gravity of the region of major wave activity from near 10°W in Fig. 24a to 15°W or beyond in Fig. 25c. The migration appears to involve a movement of the original point of maximum variance from about 9°W to about 20°W and the formation of a second maximum near 6°W at 48h that moves to 12°W at 72h. In addition, a new, minor maximum appears at 72h near 20°N, 2°W.

Charts of the variance of analysed and forecasted temperatures are shown in Fig. 25. The variance of analysed temperature (Fig. 25a) exhibits two major maxima, as noted previously. The coastal maximum persists and strengthens during the 72h period. The interior maximum near 2°E appears to migrate westward during the first 48 hours of the forecast and merge with the coastal maximum (Fig. 25b). At 72 hr a new, but weaker, maximum is in evidence at nearly the original position of the interior maximum.

Covariance patterns appear in Figs. 26-28. The major feature of the u-v covariance pattern (Fig. 26a) is the already remarked on dipole structure with negative flux centred near 18°N, 8°W and positive flux near 8°N, 10°W. During the 72 h forecast interval the pattern weakens markedly and migrates westward (Fig. 27c). Curiously, at 72 hours there is indication that the dipole pattern is being reestablished between 0°W and 5°W.

The v-T covariance or meridional heat flux (Fig. 27) exhibits little, if any, overall change of intensity during the 72 h forecast interval. However, individual maxima migrate westward and undergo quite large changes in strength. The maxima in question are denoted by the letters A-D in Figs. 27a-c. Maximum A moves from 18°W to 32°W during the 3 days and weakens considerably. Maxima B and C, on the other hand, display strong

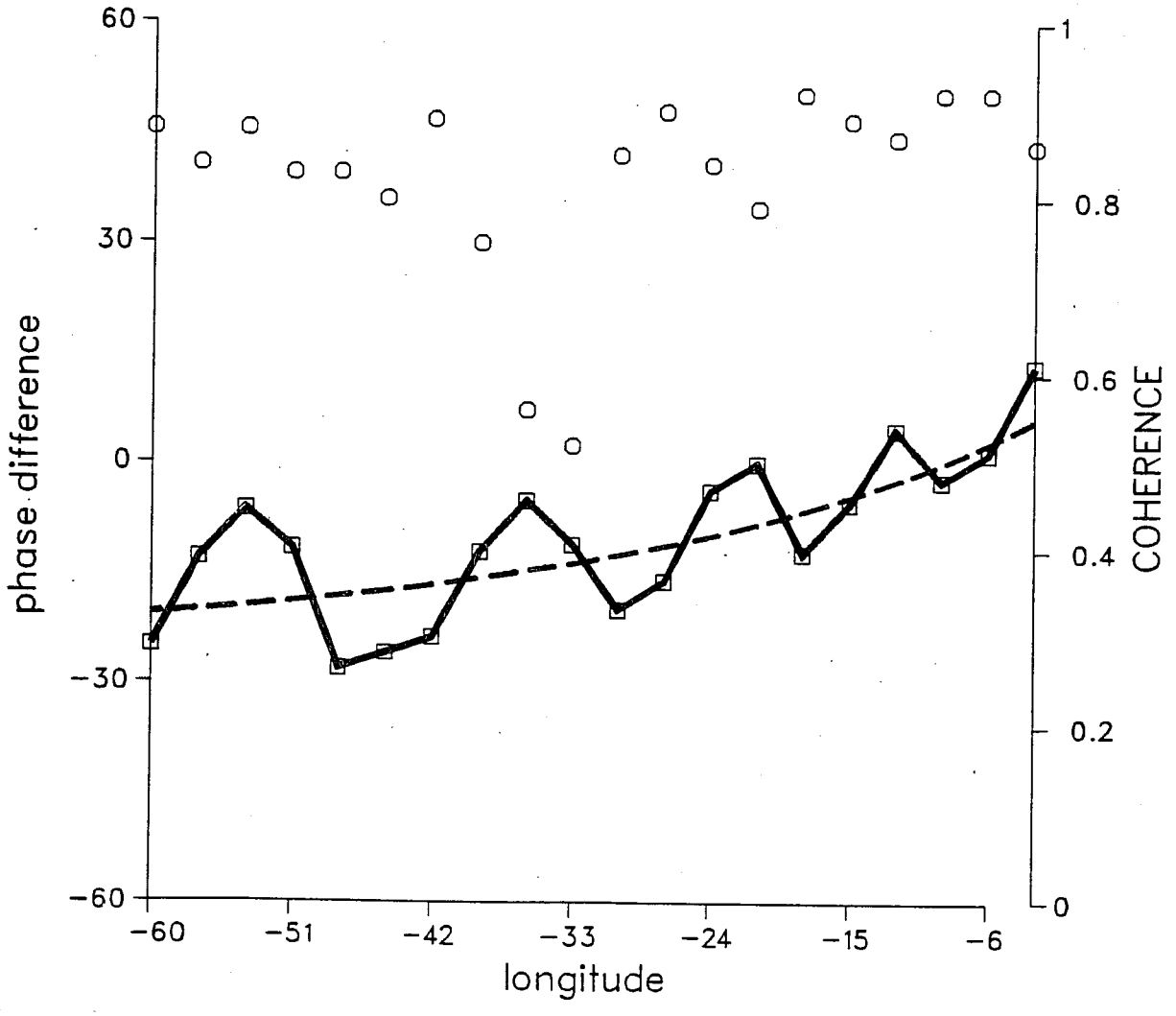

Figure 23 Phase differences (squares) and coherence (circles) between time series of analysed 850 mb winds and corresponding 48 h forecasted winds at various longitudes along 18°N. Broken line gives smoothed depiction of phase/longitude relationship. See text for further explanation.

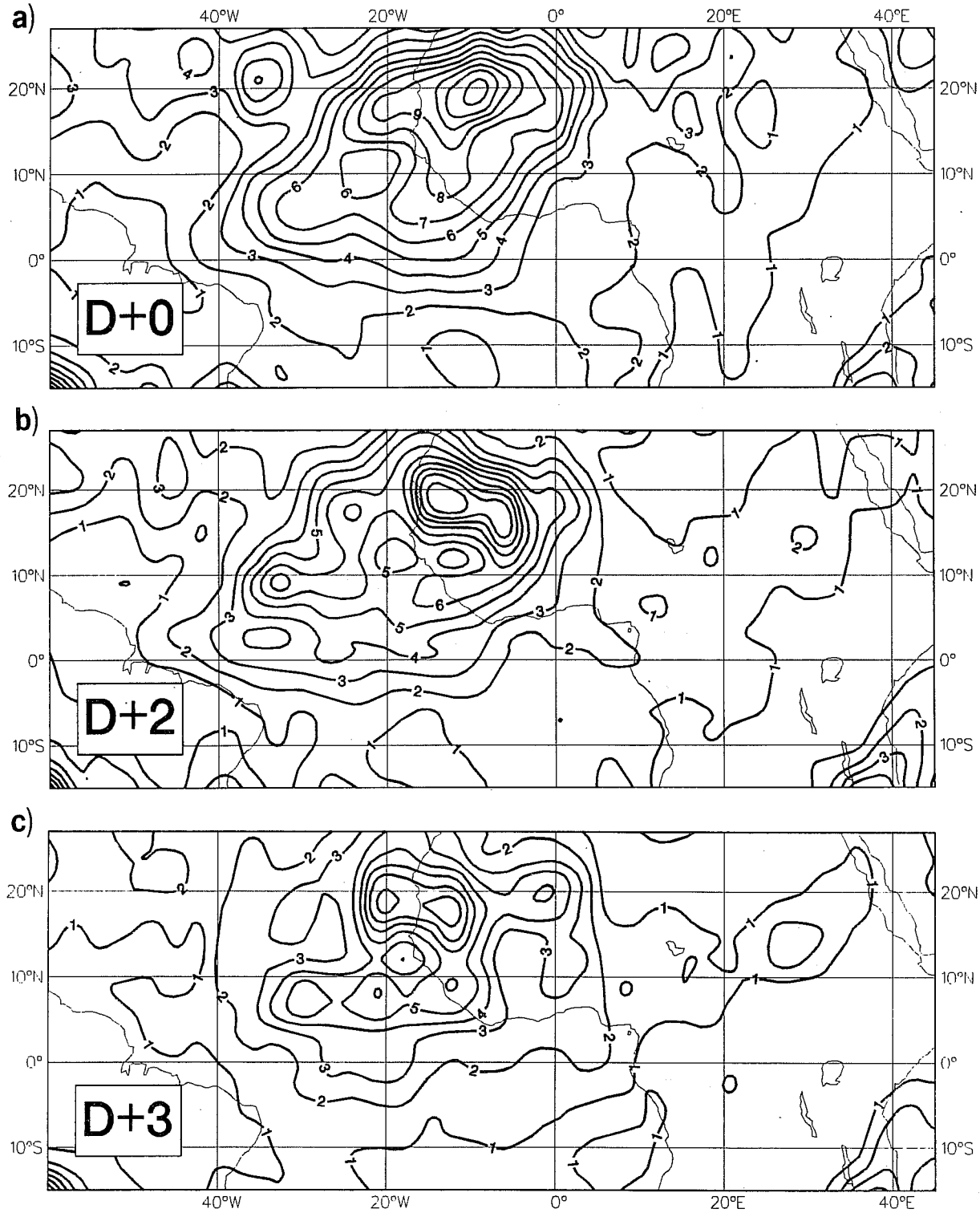

Figure 24 (a) Analysed, (b) 48 h forecasted and (c) 72 h forecasted variance fields of meridional wind at 850 mb for August-September 1985. Units: $m^2\ s^{-2}$.

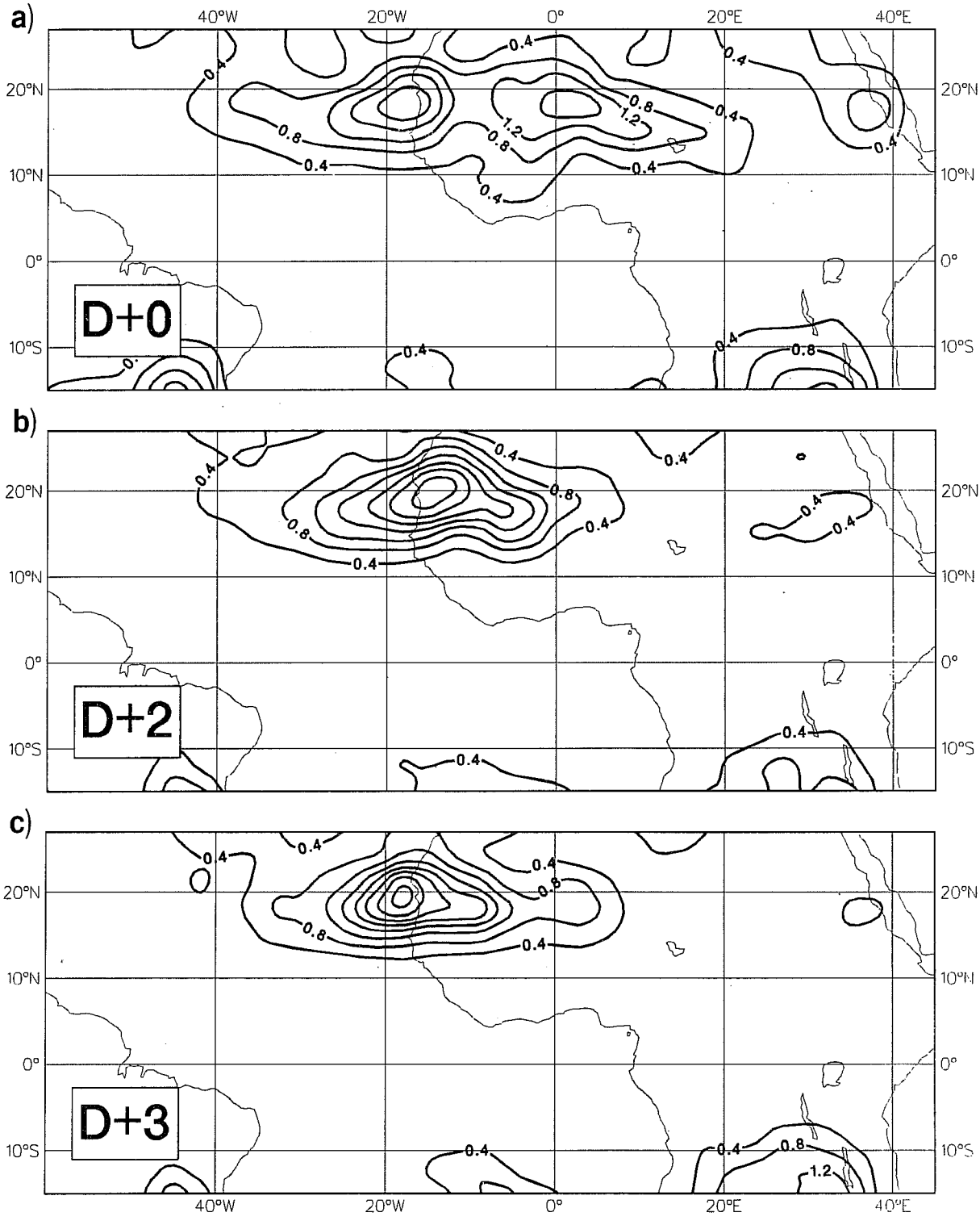

Figure 25 As in Fig. 24 except for temperature. Units: $[°C]^2$.

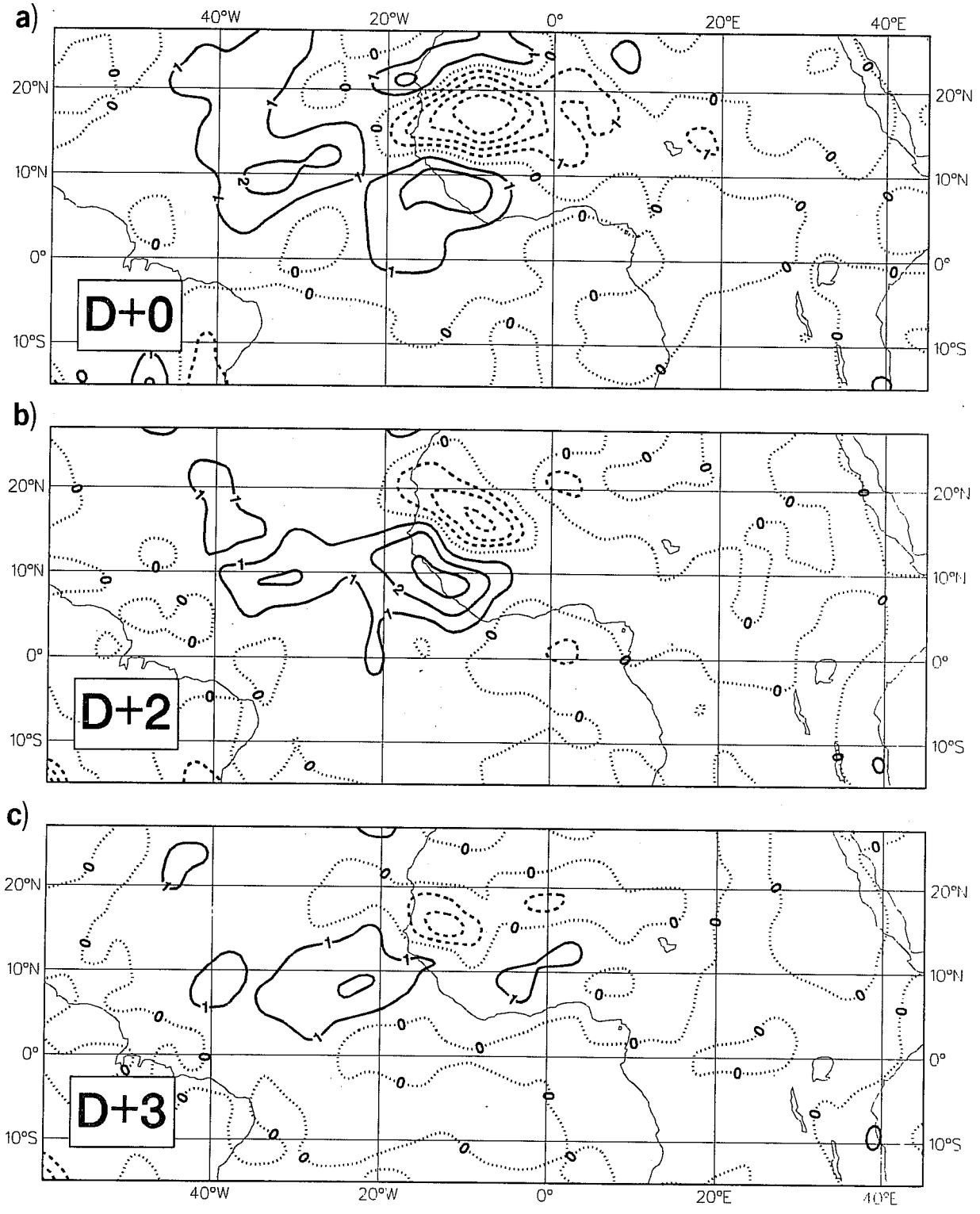

Figure 26 As in Fig. 24 except for covariance of zonal (u) and meridional (v) wind components. Units: $m^2\ s^{-2}$.

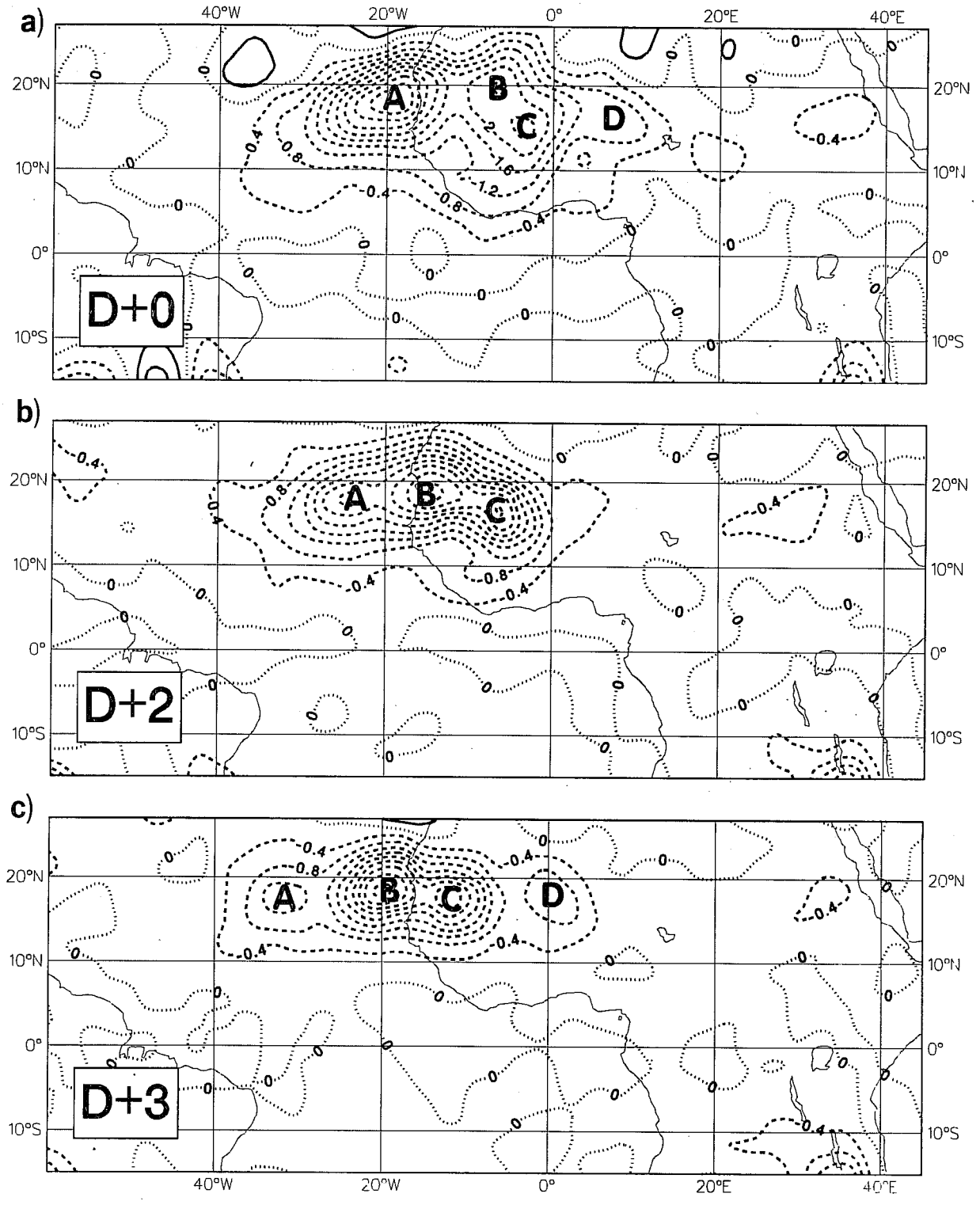

Figure 27 As in Fig. 26 except for meridional wind and temperature. Units: ms^{-1} °C.

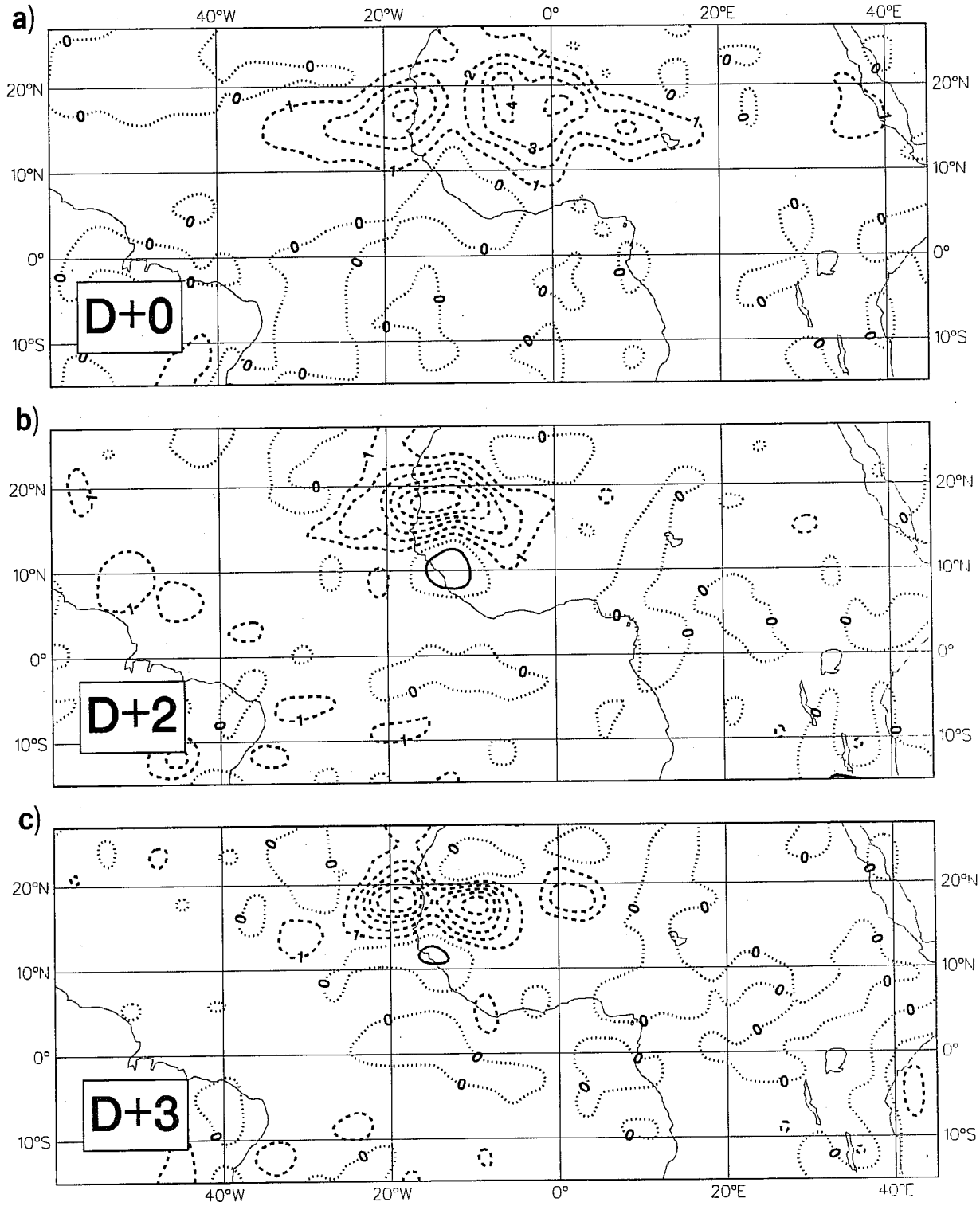

Figure 28 As in Fig. 26 except for vertical velocity (ω) and temperature. Units: 10^{-2} Pa s^{-1} °C.

intensification as they migrate to or towards the position of the original major maximum (A in Fig. 27a). D first appears as a distinct maximum in the 72h forecasts. It, too, is conceivably a westward-propagating intensifying feature.

The ω-T covariance (Figs. 28a-c) shows a tendency for the area of negative covariance (conversion of eddy available to eddy kinetic energy) to shrink during the 3 day period while individual centres increase in intensity. The westward migration of the centres is evident as is the weakening of the westernmost centre and the development, or redevelopment, of the easternmost.

On the whole the results of the comparison of analysed and forecast variance fields in the 3-5 day frequency band support the conclusions of Part I that the 48 h forecasts represent the observed waves at 850 mb with encouraging fidelity and possess considerable skill. The present results for the statistics of the 72 h forecasts suggest that it may be well worthwhile investigating the forecast skill at this range also.

8. SUMMARY AND DISCUSSION

8.1 Summary

In Part I of this study synoptic methods were used to evaluate the performance of the ECMWF system in analysing and forecasting easterly wave disturbances over Africa and the tropical Atlantic during August-September 1985. In this second part of the study, standard spectral methods are employed for the purpose of confirming and extending the previous results. The analysis is based on twice-daily gridded data from the operational archives. As background to the study, various time-mean fields were prepared for the two month period. These include: horizontal maps of the 1000, 850, 700 and 200 mb flow, 850 and 700 mb vorticity, 1000 mb divergence, and 1000, 850, 700 and 500 mb specific humidity; and meridional cross sections along 40°W, 20°W, 0° and 20°E of the horizontal wind components (u,v), vertical motion (ω), divergence (D), vorticity (ζ) temperature (T) and specific humidity (q). Important climatological features such as the southwest monsoon, trade winds, ITCZ, African Easterly Jet (AEJ) and Tropical Easterly Jet are well depicted by the time-mean fields despite the data deficiencies documented in Part I.

Spectra of time series of the 850 mb meridional wind at points along 18°N and 9°N reveal that the most prominent spectral peaks occurred in the 0.2 - 0.3 d^{-1} frequency band in agreement with the 3-5 day period found in Part I (and in many other studies of African easterly waves). The 3-5 day wave signature first appeared at approximately 10°E, as in the GATE period (June 28 - September 19, 1974), and extended westward to 60°W and beyond. At certain longitudes double peaks appeared within the 3-5 day frequency band that are believed to be dual manifestations of the primary easterly wave. However, the 5-6 day component of a double peak found near 20°N in the Atlantic is believed to be the signature of low-level disturbances that are known to form in conjunction with developments in the upper-tropospheric mid-ocean trough. Cross spectrum analysis revealed that the wave lengths of the African easterly waves were in the range 2500-2700 km, a figure that is in good agreement with, though somewhat larger than, the synoptically determined wave lengths.

Patterns of the 850 mb and 700 mb vorticity variance in the 3-5 day wave band suggest disturbance tracks and regions of wave origin that are in agreement with the synoptic findings. Meridional wind, temperature, vertical velocity and specific humidity variances and ω-T, v-T, u-v and ω-q covariances for

850 mb also reveal distinctive features of the wave behaviour. Variances and covariances at this level are especially large at the latitude of the ITCZ or monsoon trough (15°N-20°N), and the energy conversions implied by the ω-T and v-T covariances are characteristic of those occurring in amplifying baroclinic waves. Thus confirmation is given to the idea that African waves owe their origin, at least in part, to baroclinic instability of the AEJ. Comparison of the patterns of 850 mb meridional wind variance and 850 mb v-T covariance for August-September 1985 with those for the years 1981, 1982, 1983 and 1984 reveals that the major features are repeated yearly but that some variations do occur. The inter-annual variations are believed to be real, since they cannot be correlated with differences in data availability, or for the most part, with model changes.

The three-dimensional wave structure is examined with the help of meridional cross sections of variances and covariances at 9°W and vertical profiles of phases and amplitudes of various wave parameters for three locations between 9°N and 21°N along 18°W. Phases are expressed relative to the phase of the 850 mb meridional wind; vertical profiles of coherences are used to identify significant relationships. Extensive comparison is made with wave structures observed during GATE. In general the analysed structures resemble closely the structures documented by GATE investigators. The waves can be described as a two-component system characterised (1) by a northern component that forms near and poleward of the AEJ, in the vicinity of the monsoon trough, and that has the nature of a moderately shallow baroclinic disturbance and (2) by a southerly component that forms in the vicinity of the equatorial rain belt near 10°N and that derives its energy from latent heat release in cumulus convection. Evidence was found of a substantial barotropic energy conversion associated with a pronounced positive momentum flux at middle levels equatorward of the AEJ. The region of barotropic energy conversion was more closely linked to the main region of wave growth than during Phase III of GATE, lending support to the idea that barotropic instability also plays a role in the wave development.

Cross spectrum analysis between time series of analysed and forecast 850 mb meridional winds confirmed the previous finding that forecasted wave speeds were somewhat slower than the analysed wave speeds. The 48 h longitudinal displacement error, however, was only 150 km or less for a typical

longitudinal displacement of 1400 km. Comparison of the variance and covariance fields of the analyses with the variance and covariance fields of the 48h and 72h forecasts revealed that the 3-5 day wave fields were preserved with varying degrees of fidelity. The variance of the meridional component diminished considerably during the 72h period, as did the covariance of u and v. The temperature variance, on the other hand, increased slightly during the interval. The regions of largest v-T and ω-T covariance shrank in size, but central intensities strengthened markedly. For reasons that are not understood, many features of the variance and covariance patterns propagated westward during the forecast period and were replaced by similar features that reformed to the east.

8.2 Discussion

The present paper and its companion synoptic study (Part I) constitute the most detailed study to date of the ability of the ECMWF analysis/forecast system to analyse and forecast tropical disturbances using operational data. Because of the extensive literature on the GATE area, we have concentrated on West Africa and the tropical Atlantic.

Detailed investigation of the analysed fields provides clear evidence of the ability of a modern data assimilation system to make coherent physical sense of sparse and heterogeneous observations. The forecast model is crucial to this capability, through the accuracy of the numerics and the verisimilitude of the physical parameterisations.

Painstaking comparison of the analysed fields with the GATE data show considerable similarities between the data sets, both in the mean fields and in the structure of the transient easterly disturbances. Some minor differences were identified in the structure of the easterly waves. We are uncertain if these are due to defects of the convection scheme, or reflect real inter-annual differences. The analyses for the last five years evince marked inter-annual variations in wave activity. Some of this may be due to model changes, but much of it must be real. The relationship of these variations to changes in seasonal rainfall deserves investigation.

The preservation of the wave structures in the 48 h and 72 h forecasts has been documented in this paper. Taken with the evident success of the 48 h

forecasts documented in Part I, we have reliable evidence that skilful forecasts for tropical easterly waves are now possible with operational data. Improvements in data availability would certainly improve the reliability of the analyses and forecasts. Some of the data deficiencies may be remediable. Improved wind retrieval algorithms ought to improve the yield of low-level cloud track winds over the ocean.

We have concentrated our efforts on the dynamical fields, particularly wind, and have largely ignored the precipitation field. Ongoing studies are addressing the problem of precipitation forecasting. Given the difficulties of modelling tropical convection, it is anticipated that precipitation forecasts based on statistical interpretation of model wind fields may prove more useful than forecasts based directly on the model.

The results of this study are only valid for the Atlantic-African region. Similar studies are needed for the Indian Ocean and Pacific Ocean regions. It is known that some important aspects of model behaviour vary between the regions (Tiedtke et al., 1987). There are also large variations in data availability between the regions. The results of the global study of Nitta and Takayabu (1985), and the regional evaluation of the Malaysian Weather Service (WMO, 1986), give grounds for optimism that routine forecasting by numerical methods may prove useful for wide areas of the tropics.

References

Albignat, J.P. and R.J. Reed, 1980: The origin of African wave disturbances during Phase III of GATE. Mon.Wea.Rev., 108, 1827-1839.

Burpee, R.W., 1972: The origin and structure of easterly waves in the lower troposphere of North Africa. J.Atmos.Sci., 29, 77-90.

Burpee, R.W., 1975: Some features of synoptic-scale waves based on compositing analysis of GATE data. Mon.Wea.Rev., 103, 921-925.

Carlson, T.N., 1969: Some remarks on African disturbances and their progress over the tropical Atlantic. Mon.Wea.Rev., 97, 716-726.

Carlson, T.N. and J.M. Prospero, 1972: The large-scale movement of Saharan air outbreaks over the Northern Equatorial Atlantic. J.Appl.Meteor., 11 283-297.

Frank, N., 1969: The "inverted V" cloud pattern-an easterly wave? Mon.Wea.Rev., 97, 130-140.

Jarraud, M., A.J. Simmons and M. Kanamitsu, 1985: Development of the high resolution model. ECMWF Tech. Memo. 107. Reading, UK, 61 pp.

Klinker, E. and M. Capaldo, 1986: Systematic errors in the baroclinic waves of the ECMWF mode. Tellus, 38A, 215-235.

Lindzen, R.S., 1974: Wave-CISK in the tropics. J.Atmos.Sci., 156-179.

Mass, C., 1979: A linear primitive equation model of African wave disturbances. J.Atmos.Sci., 36, 2075-2092.

Mouzna, N., 1984: Les caracteristiques de propagation des ondes tropicales en Afrique de L'ouest observces pendant l'experience WAMEX, Thesis, University of Clermont, 52pp.

Nitta, T., and Y. Takayabu, 1985: Global analysis of the lower tropospheric disturbances in the tropics during the northern summer of the FGGE year. Part II: Regional characteristics of the disturbances. Pure Appl. Geophys., 123, 272-292.

Norquist, D.C., E.E. Recker and R.J. Reed, 1977: The energetics of African wave disturbances as observed during Phase III of GATE. Mon.Wea.Rev., 105, 334-342.

Reed, R.J., 1978: The structure and behaviour of easterly waves over West Africa and the Atlantic. Meteorology over the Tropical Oceans, Roy.Meteor.Soc., Bracknell, United Kingdom, 57-71.

Reed, R.J., D.C. Norquist and E.E. Recker, 1977: The structure and properties of African wave disturbances as observed during Phase III of GATE. Mon.Wea.Rev., 103, 317-333.

Reed, R.J., A. Hollingsworth, W.E. Heckley and F. Delsol, 198: An evaluation of the performance of the ECMWF operational forecasting system in analysing and forecasting tropical easterly wave disturbances. Part I: Synoptic Investigation.

Rennick, M.A., 1976: The generation of African waves. J.Atmos.Sci., 33, 1955-1969.

Shaw, D., P. Lönnberg, A. Hollingsworth and P. Unden, 1987: The 1984/85 revisions of the ECMWF analysis system. To appear in Quart.J.Roy.Meteor.Soc.

Simmons, A.J., 1977: A note on the instability of the African easterly jet. J.Atmos.Sci., 34, 1670-1674.

Simpson, R.H., N. Frank, D. Shideler and H.M. Johnson, 1968: Atlantic tropical disturbances, 1967. Mon.Wea.Rev., 96, 251-259.

Thompson, R.M., Jr., S.W. Payne, E.E. Recker and R.J. Reed, 1979: Structure and properties of synoptic scale wave disturbances in the intertropical convergence zone in the eastern Atlantic. J.Atmos.Sci., 36, 53-72.

Tiedtke, M., W.A. Hekcley, J. Slingo, A. Simmons, M. Jarraud, G. Sommeria, 1987: Tropical forecasts at ECMWF: Impacts of revised physics and increased horizontal resolution. To be submitted.

Viltard, A. and P. de Félice, 1979: Statistical analysis of wind velocity in an easterly wave over West Africa. Mon.Wea.Rev., 107, 1320-1327.

WMO, 1986: Preliminary assessment of ECMWF products used in Malaysia. WMO Bulletin, 35, 237-240.

Yanai, M., T. Maruyama, T. Nitta and Y. Hayashi, 1968: Power spectra of large-scale disturbances over the tropical Pacific. J.Meteor.Soc.Japan., 46, 308-323.

Appendix A

The following figures, referenced in the text and in Table 1, are taken from the paper "The Origin of African Wave Disturbances During Phase III of GATE" by Albignat and Reed (1980) and from the thesis "The Propagation Characteristics of West African Tropical Waves Observed During WAMEX" by Mouzna (1984).

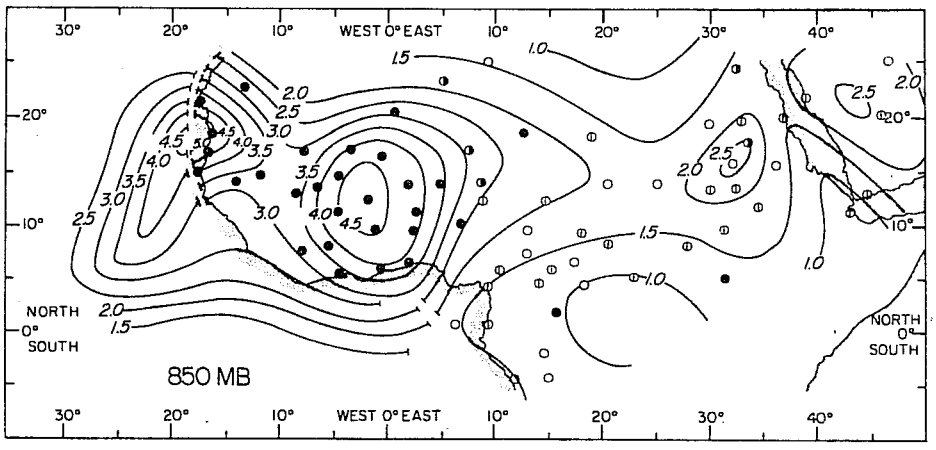

FIG. 3. Amplitude of meridional wind oscillation (m s^{-1}) in the frequency band 0.2–0.4 cpd at 850 mb. Isopleths over land are based on 28-day period of record, over the ocean on 21-day period. Solid circle signifies a pronounced spectral peak in the 0.2–0.4 cpd band, half solid circle a secondary peak, circle with line a weak peak, open circle no detectable peak.

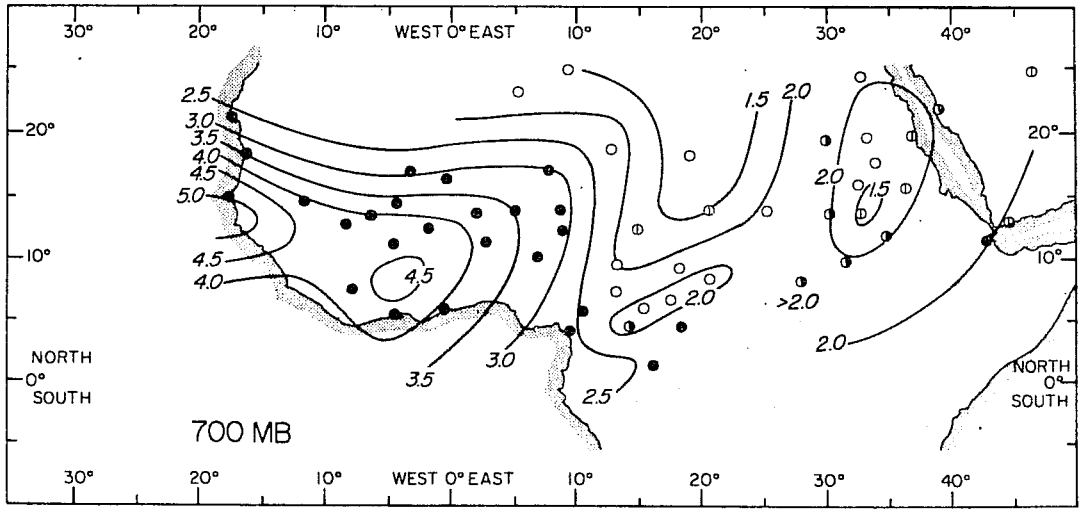

FIG. 7. Amplitude of meridional wind oscillation in 0.2–0.4 cpd frequency band at 700 mb. See Fig. 3 for further explanation.

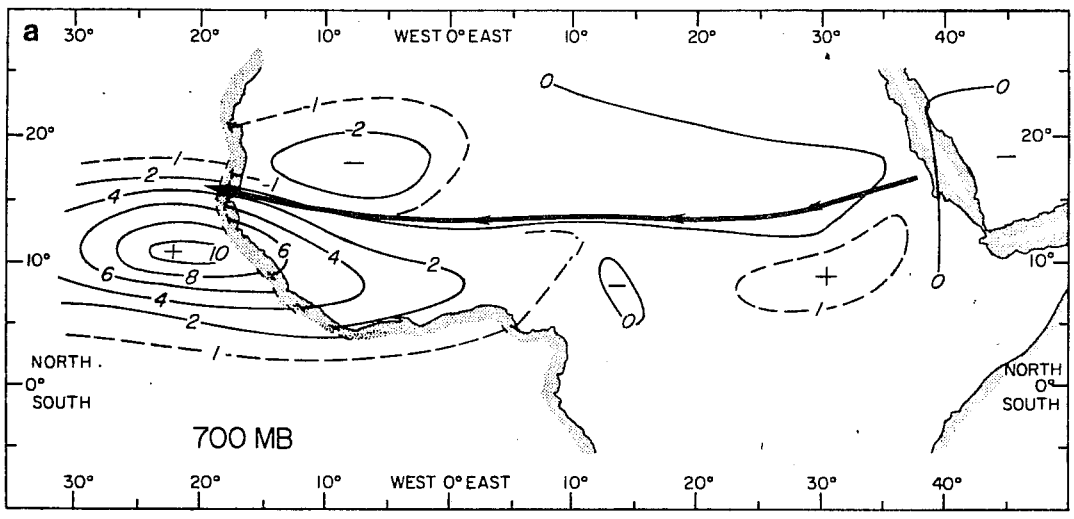

FIG. 10. (a) Northward flux of zonal momentum ($\overline{u'v'}$) at 700 mb in 0.2–0.4 cpd frequency band. Units: $m^2\ s^{-2}$. Heavy line represents jet stream axis. Isopleths over land are based on 28-day period of record, over the ocean on 20-day period.

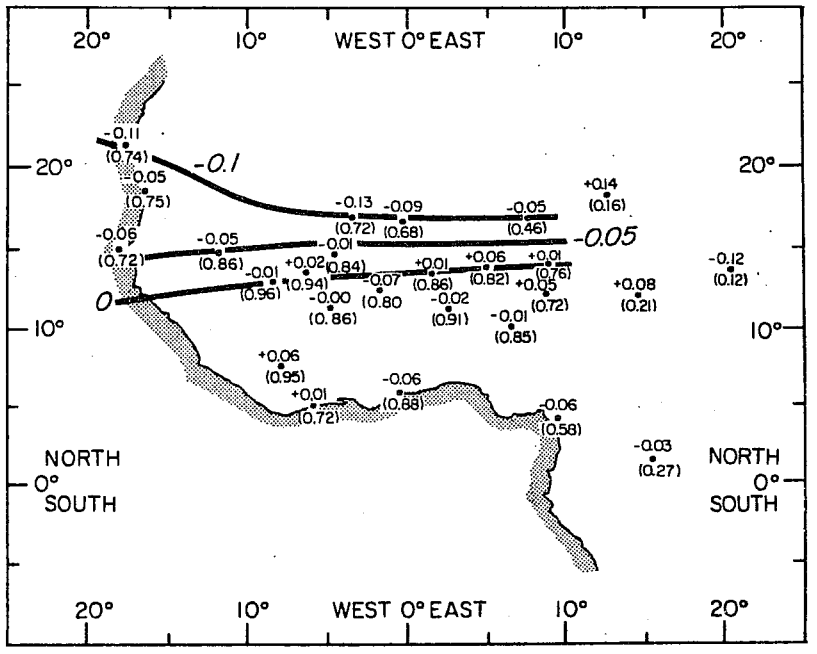

FIG. 12. Phase difference in cycles between meridional wind oscillations at 850 and 700 mb for 0.2–0.4 cpd frequency band. Numerical values are plotted above station. Coherence squares are shown in parentheses. A positive (negative) difference indicates a westward (eastward) tilt with height.

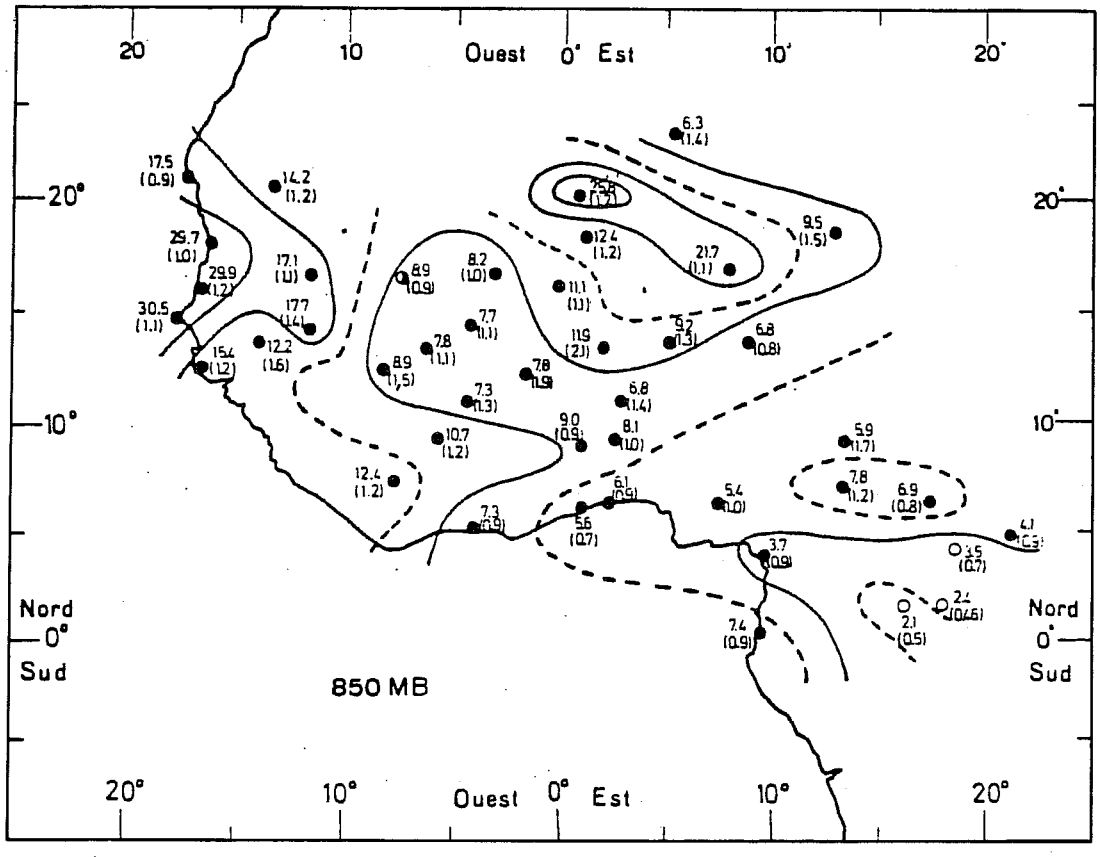

Figure 14-a : Variance de la composante méridienne du vent dans la bande de fréquence de 0,2 à 0,4 cycle par jour. Le rapport de cette variance sur celle de la bande de fréquence de 0,06 à 0,26 cpj est indiqué entre parenthèses.
Les cercles noirs représentent les stations qui ont un pic net entre 0,2 et 0,4 cpj et les cercles évidés celles qui n'en ont pas, à 850 mb. (from Mouzna, 1984)

Appendix B

The following figures, referenced in Table 1, are taken from the paper "The Structure and Properties of African Wave Disturbance as Observed During Phase III of GATE" by Reed, Norquist and Recker (1977).

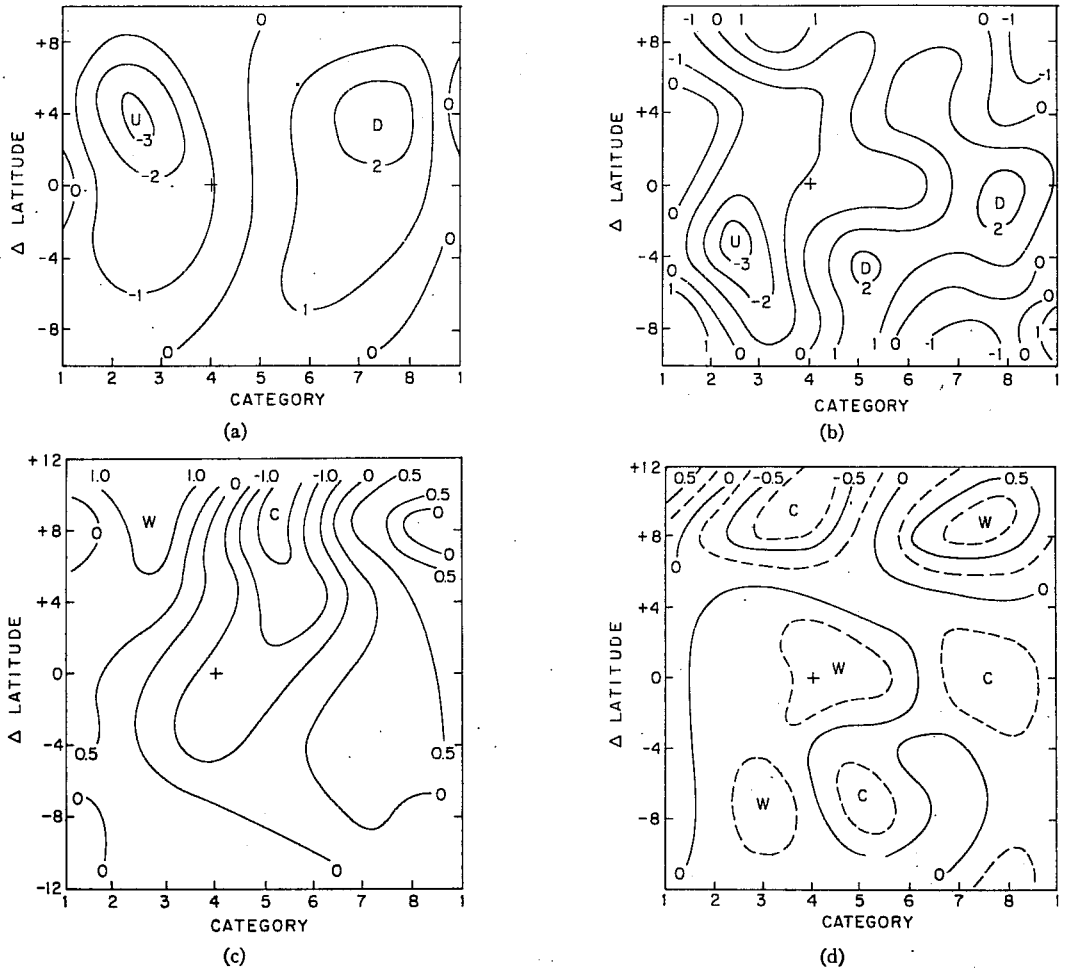

FIG. 7. Vertical motion deviation (mb h^{-1}) from zonal mean at (a) 850 mb, (b) 300 mb; temperature deviation (°C) at (c) 850 mb, (d) 300 mb
300 mb.

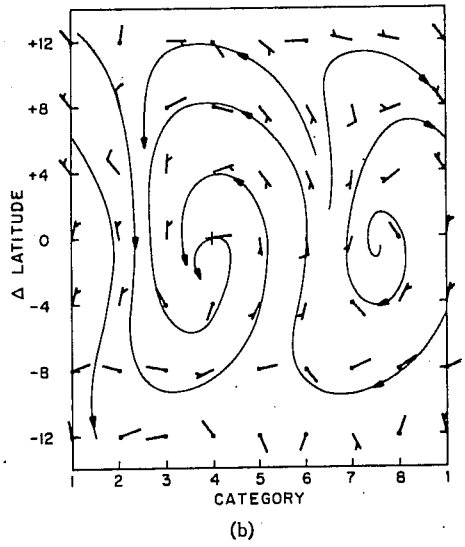

FIG. 4. Streamlines for perturbed wind field.
(b) 850 mb.

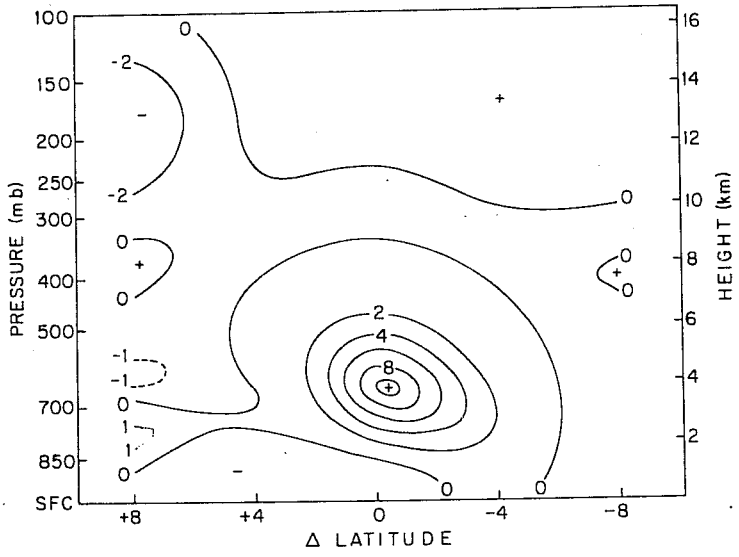

FIG. 2. Meridional distribution of $-[u'v']\partial[u]/\partial y$ for the combined region. Units are 10^{-5} m^2 s^{-3} (or W kg^{-1}).

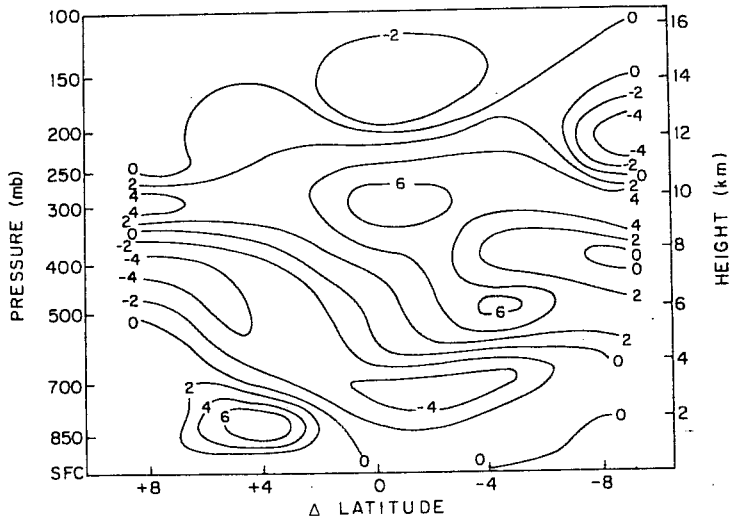

FIG. 3. Meridional distribution of $-R\bar{p}^{-1}[\omega'T']$ for the combined region. Units are 10^{-5} m^2 s^{-3} (or W kg^{-1})

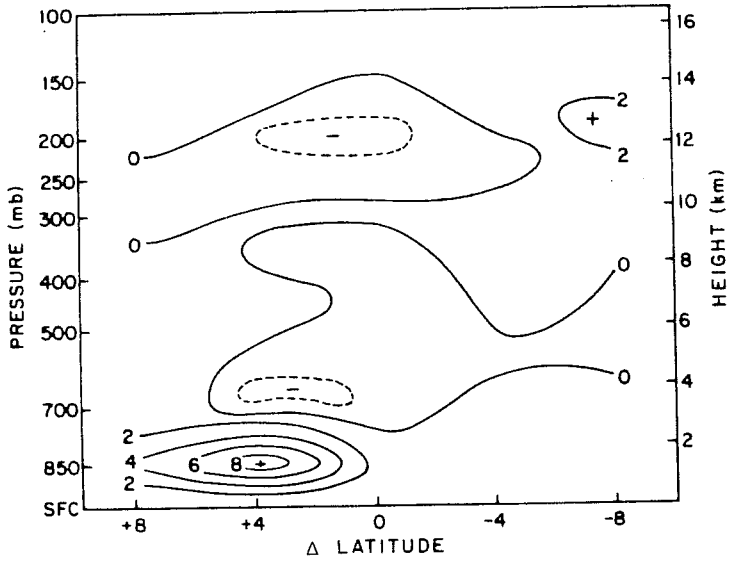

FIG. 4. Meridional distribution of $-g\bar{\sigma}^{-1}[v'T']\partial[T]/\partial y$ for the combined region. Units are 10^{-5} m^2 s^{-3}.

ECMWF PUBLISHED TECHNICAL REPORTS

No.1 A case study of a ten day prediction. (Arpe, K., L. Bengtsson, A. Hollingsworth and J. Janjic; September, 1976)

No.2 The effect of arithmetic precisions on some meteorological integrations. (Baede, A.P.M., D. Dent and A. Hollingsworth; December 1976)

No.3 Mixed-radix fast Fourier transforms without reordering. (Temperton, C.; February, 1977)

No.4 A model for medium-range weather forecasting - adiabatic formulation. (Burridge, D.M., and J. Haseler; March 1977)

No.5 A study of some parameterisations of sub-grid processes in a baroclinic wave in a two-dimensional model. (Hollingsworth, A.; July, 1977)

No.6 The ECMWF analysis and data assimilation scheme: analysis of mass and wind field. (Lorenc, A., I. Rutherford and G. Larsen; December, 1977)

No.7 A ten-day high-resolution non-adiabatic spectral integration; a comparative study. (Baede, A.P.M., and A.W. Hansen; October, 1977)

No.8 On the asymptotic behaviour of simple stochastic-dynamic systems. (Wiin-Nielsen, A.; November, 1977

No.9 On balance requirements as initial conditions. (Wiin-Nielsen, A.; October, 1978)

No.10 ECMWF model - parameterization of sub-grid scale processes. (Tiedtke, M., J.-F. Geleynn, A. Hollingsworth and J.-F. Louis; January, 1979)

No.11 Normal mode initialization for a multi-level grid-point model. (Temperton,C., and D. L. Williamson; April, 1979)

No.12 Data assimilation experiments. (Seaman, R.; October, 1978)

No.13 Comparison of medium range forecasts made with two parameterization schemes. (Hollingsworth, A., K. Arpe, M. Tiedtke, M. Capaldo, H. Savijärvi, O. Åkesson, and J.A. Woods; 1978)

No.14 On initial conditions for non-hydrostatic models. (Wiin-Nielsen, A.C.; November, 1978)

No.15 Adiabatic formulation and organization of ECMWF's spectral model. (Baede, A.P.M., M. Jarraud and U. Cubasch; 1979)

No.16 Model studies of a developing boundary layer over the ocean. (Okland, H.; November, 1979)

No.17 The response of a global barotropic model to forcing by large-scale orography. (Quiby, J.; January, 1980)

No.18 Confidence limits for verification and energetics studies. (Arpe, K.; May, 1980)

No.19 A low order barotropic model on the sphere with orographic and Newtonian forcing. (Källén, E.; July, 1980)

No.20 A review of the normal mode initialization method. (Du H, X.Y.; August, 1980)

No.21 The adjoint equation technique applied to meteorological problems. (Kontarev, G.; September, 1980)

No.22 The use of empirical methods for mesoscale pressure forecasts. (Bergthorsson, P.; November, 1980)

No.23 Comparison of medium range forecasts made with models using spectral or finite difference techniques in the horizontal. (Jarraud, M., C. Girard, and U. Cubasch; February, 1981)

No.24 On the average errors of an ensemble of forecasts. (Derome, J.; February, 1981)

No.25 On the atmospheric factors affecting the Levantine Sea. (Ozsoy, E.; May, 1981)

No.26 Tropical influences on stationary wave motion in middle and high latitudes. (Simmons, A.J.; August, 1981)

No.27 The energy budgets in North America, North Atlantic and Europe based on ECMWF analyses and forecasts. (Savijärvi, H.; November, 1981)

No.28 An energy and angular momentum conserving finite-difference scheme, hybrid coordinates and medium-range weather prediction. (Simmons, A.J., and R. Strüfing; November, 1981)

No.29 Orographic influences on Mediterranean lee cyclogenesis and European blocking in a global numerical model. (Tibaldi, S. and A. Buzzi; February, 1982)

No.30 Review and re-assessment of ECNET - A private network with open architecture. (Haag, A., F. Königshofer and P. Quoilin; May, 1982;)

No.31 An investigation of the impact at middle and high latitudes of tropical forecast errors. (Haseler, J.; August, 1982)

No.32 Short and medium range forecast differences between a spectral and grid point model. An extensive quasi-operational comparison. (Girard, C. and M. Jarraud; August, 1982)

No.33 Numerical simulations of a case of blocking: the effects of orography and land-sea contrast. (Ji, L.R., and S. Tibaldi; September, 1982)

No.34 The impact of cloud track wind data on global analyses and medium range forecasts. (Källberg, P., S. Uppala, N. Gustafsson and J. Pailleux; December, 1982)

No.35 Energy budget calculations at ECMWF: Part I: Analyses 1980-81 (Oriol, E.; December, 1982)

No.36 Operational verification of ECMWF forecast fields and results for 1980-1981. (Nieminen, R.; February, 1983)

No.37 High resolution experiments with the ECMWF model: a case study. (Dell'Osso, L.; September, 1983)

No.38 The response of the ECMWF global model to the El-Nino anomaly in extended range prediction experiments. (Cubasch, U.; September, 1983)

No.39 On the parameterisation of vertical diffusion in large-scale atmospheric models. (Manton, M.J.; December, 1983)

No.40 Spectral characteristics of the ECMWF objective analysis system. (Daley, R.; December, 1983)

No.41 Systematic errors in the baroclinic waves of the ECMWF model. (Klinker, E., and M. Capaldo; February, 1984)

No.42 On long stationary and transient atmospheric waves. (Wiin-Nielsen, A.C.; August, 1984)

No.43 A new convective adjustment scheme. Betts, A.K., and M.J. Miller; October, 1984)

No.44 Numerical experiments on the simulation of the 1979 Asian summer monsoon. (Mohanty, U.C., R.P. Pearce and M. Tiedtke; October, 1984)

No.45 The effect of mechanical forcing on the formation of a mesosale vortex. (Wu, G.X., and S.J. Chen; October, 1984)

No.46 Cloud prediction in the ECMWF model. (Slingo, J., and B. Ritter; January, 1985)

No.47 Impact of aircraft wind data on ECMWF analyses and forecasts during the FGGE period. 8-19 November 1979. (Baede, A.P.M., P. Kållberg, and S. Uppala; March, 1985)

No.48 A numerical case study of East Asian coastal cyclogenesis. (Chen, S.J. and L. Dell'Osso; May, 1985)

No.49 A study of the predictability of the ECMWF operational forecast model in the tropics. (Kanamitsu, M.; September, 1985)

No.50 On the development of orographic cyclones. (Radinovic, D.; June, 1985)

No.51 Climatology and systematic error of rainfall forecasts at ECMWF. (S. Tibaldi; October, 1985)

No.52 Impact of modified physical processes on the tropical simulation in the ECMWF model. (Mohanty, U.C., J.M. Slingo and M. Tiedtke; October, 1985)

No.53 The performance and systematic errors of the ECMWF tropical forecasts (1982-1984). (Heckley, W.A.,; November, 1985)

No.54 Finite element schemes for the vertical discretization of the ECMWF forecast model using linear elements. (Burridge, D.M., J. Steppeler, and R. Strüfing; January, 1986)

No.55 Finite element schemes for the vertical discretization of the ECMWF forecast model using quadratic and cubic elements. (Steppeler, J.; February, 1986)

No.56 Sensitivity of medium-range weather forecasts to the use of an envelope orography. (Jarraud, M., A.J. Simmons and M. Kanamitsu; September 1986)

No.57 Zonal diagnostics of the ECMWF 1984-85 operational analyses and forecasts. (Brankovic, C.; October, 1986)

No.58 An evaluation of the performance of the ECMWF operational forecasting system in analysing and forecasting tropical easterly wave disturbances. Part 1: Synoptic investigation. (Reed, R.J., A. Hollingsworth, W.A. Heckley and F. Delsol; September, 1986)

No.59 Diabatic nonlinear normal mode initialisation for a spectral model with a hybrid vertical coordinate (Wergen, W.; December 1986).

No.60 An evaluation of the performance of the ECMWF operational forecasting system in analysing and forecasting tropical westerly wave disturbances. Part 2: Spectral investigation. (Reed, R.J., E. Klinker and A. Hollingsworth; September 1986).